Photophysical properties of chiral semiconductor nanocrystals in biological environments

School of Electrical Engineering

Thesis submitted for examination for the degree of Master of Science in Technology.

Espoo 19.06.2016

Thesis supervisor:
Associate Professor Zhipei Sun

Author: Ilia Litvinov

Title: Photophysical properties of chiral semiconductor nanocrystals in biological environments

Date: 19.06.2016 Language: English Number of pages: 76

Department of Micro- and Nanosciences

Professorship: S-104

Supervisor: Associate Professor Zhipei Sun

During the last decade much work has been focused on the use of nanostructures toward problems of biology and medicine. The issue of nanostructures application in cancer therapy depends on the effectiveness of the nanocrystals loading into cells. In this work chiral nanostructures based on CdSe/ZnS quantum dots (QD) and CdSe/CdS quantum dots in quantum rods (DiR) solubilized by L- and D-cysteine were formed using phase transfer method. We studied photophysical properties of chiral nanostructures in different biological media and analyzed spectral luminescent properties of complexes based on chiral nanostructures. Enantioselective cellular uptake of nanostructures was revealed, namely that L-cysteine capped nanocrystals uptake is higher than that of D-cysteine capped nanocrystals. Enantioselective interaction between chiral enantiomers of molecules and chiral nanostructures was detected. We believe this principle may lay the groundwork for novel approaches to studying biological objects and to application of nanostructures in medicine.

Keywords: nanocrystals, quantum dots, dot-in-rods, chirality, cancer

Preface

I want to thank Dr. Anna Orlova and all my colleagues from the department of Optical Physics and Modern Natural Science in ITMO University.
Many thanks to Prof. Markku Sopanen and Prof. Zhipei Sun for their good guidance.

Contents

Symbols and abbreviations

Symbols

C	concentration
d	nanostructure core diameter
D	optical density
E_t	transfer efficiency
I	intensity (luminescence)
k_r	energy transition radiative constant
n	refractive index
$N = 6{,}022 \cdot 10^{23}$ mol^{-1}	Avogadro constant
N_{abs}	number of absorbed quanta
N_{emit}	number of emitted quanta
QY_{0D}	donor luminescence quantum yield without a quenching agent
R_0	distance between a donor and an acceptor at which the energy transfer efficiency by FRET mechanism is 50%
R_{DA}	distance between a donor and an acceptor
ε	extinction coefficient
λ	wavelength
τ	luminescence lifetime
$\langle\tau\rangle$	mean luminescence lifetime
φ	quantum yield
$\Phi^2 = {}^2/_3$	orientation factor

Abbreviations

Ce6 chlorin e6

DiR quantum dot in quantum rod

EAC Ehrlich ascites carcinoma

FRET Förster resonance energy transfer

NC nanocrystal

QD quantum dots

QR nanorod, quantum rod

1 Introduction

Chirality is mainly related to symmetry of molecules. A lack of violation of symmetry is referred to as asymmetry. Asymmetry can be found on different levels of matter. The objects are chiral, if they cannot be superposed with their mirror image.

Chirality is a typical characteristic of most biologically active molecules, and is responsible for their stereo aspects when these molecules interact the surrounding medium. Chirality is also one of the key factors for molecular recognition that has many applications in chemistry and biology.

Currently, huge research efforts have been focused on chirality research. Scientists have conducted experiments to modify the surfaces of nanostructures. Chiral nanostructures can be obtained by using chiral molecules as stabilizers in colloid synthesis or as ligands in post-synthesis phase transfer.

There is a theory that these chiral properties of quantum dots may affect their ability of interacting with biomolecules. As we know the most important elements of living organisms, the amino acids and nucleic acids, possess chiral properties. So, chirality can modulate several vital processes in the living cells. Chirality of nanostructures can also affect their uptake by biological objects, for example, cancer cells.

CdSe/ZnS nanocrystals are often used in such studies because of their bright and stable photoluminescence. In this work chiral nanostructures based on CdSe/ZnS quantum dots (QDs) and CdSe/CdS quantum dots in quantum rods (DiRs) solubilized by L- and D-cysteine were formed using phase transfer method. When studying chiral nanostructures, the most precise attention is given to their photophysical properties, because these properties play a key role for various potential applications, such as in disease diagnostics and treatment. Another important issue is the complexes of nanostructures with tetrapyrrole molecules, which also possess chirality.

The goal of this work is formation of chiral nanostructures and investigation of their photophysical properties in different biological media, including the living cells of Ehrlich ascites carcinoma.

The first chapter of this dissertation contains an analytical literature review dedicated to main properties of different nanostructures and complexes based on them, as well as their applications in biomedicine.

The second chapter describes the materials, equipment and methods that were used for spectral-luminescent analysis of chiral nanostructures and complexes based on nanocrystals and photosensitizer molecules.

The third chapter is devoted to studying the optical properties of chiral semiconductor nanocrystals.

In the fourth chapter, we study the problem of penetrating the living cells of Ehrlich ascites carcinoma by chiral nanostructures and estimate the influence of nanostructure chirality type on the efficiency of intracellular penetration.

The fifth chapter is dedicated to studying photophysical properties of complexes formed by chiral nanostructures and tetrapyrrole compound molecules – chlorin e6.

2 Background

2.1. Nanostructures

Nanostructures are usually considered as particles less than 100 nm in dimension. This type of structures has been used in an increasing number of different applications, including drug delivery [1]. Another issue of increasing importance is application of fluorescent semiconductor nanocrystals (quantum dots (QDs), nanorods (QRs), quantum dots in quantum rods (DiRs), dendrimers) as objects that can be used in therapy, bioengineering and medical examination [2].

2.1.1. Types of nanostructures

Today the processes of hierarchic self-organization play an important role in nanotechnology and photonics. Colloid nanoparticles stabilized by ligands are an excellent example of hierarchic order self-organization. The core of non-organic nanoparticle determines the properties of the formed structure; in turn the surface ligands define interaction of the structure with external medium [3]. Understanding these processes of interactions will lead to practical implementation of "bottom-up" nanotechnologies as an alternative to "top-down" type nanotechnologies (nanolithography, molecular beam epitaxy and others) [4].

Ligand-stabilized colloid nanoparticles, self-organized into one- two- or three-dimensional nanostructures with unique optical, electronic and magnetic properties by electrostatic, Van-der-Waals and other forms of interaction, have been demonstrated very recently [5].

Among different kinds of colloid nanostructures, the quantum dots (QD) are the most studied ones due to their simple fabrication, tunable light emission in visible and near infrared spectral regime, as well as a wide range of applications, from light

emitting diodes to biological marking [6,7,8]. Quantum dots normally belong to binary and doped semiconductor materials of groups II-VI, III-V and IV-VI with sizes of ~2-20 nm in three dimensions.

Controlled synthesis technology allows changing the nanoparticle form using nanocrystal anisotropy. Crystal structure characteristics of a particular material defines the direction of growth, which in turn affects the nanocrystal form [9,10]. This is how nanorods or tetrapods – nanocrystals stretched in four directions – are made. A shell applied on the nanostructure core changes the crystal shape in a similar way. Particularly, nanostructures of "quantum dot in quantum rod" type (DiR) are fabricated in the process of rod-shaped shell growth over a spherical core [11].

2.1.2. Photophysical properties of nanostructures

Semiconductor nanocrystals with sizes less than the exciton Bohr radius represent an intermediate class of materials between molecular and macroscopic forms of matter. In such nanocrystal an electron and a hole act as in a three-dimensional potential well; quantum confinement of both the electron and hole in all three dimensions leads to an increase of the effective band gap of the material, as the crystal size decreases [12]. Similarly to transitions between energy levels in an atom, a photon can be emitted or absorbed during charge carrier transitions between energy levels in nanocrystals [13]. Therefore, a decrease in quantum dot size leads to a blue spectral shift (to higher energy band). This process observed for both quantum dots optical absorption and emission. The transition frequencies, i.e. absorption or luminescence wavelengths, can be tuned by altering the nanocrystal size. Apart from this, the nanocrystals possess unique optical properties, such as wide absorption spectrum, as well as relatively high extinction coefficients and photoluminescence quantum yields.

2.1.3. Synthesis of semiconductor colloid nanostructures

Composite core/shell semiconductor nanostructures possess unique properties, making them promising from both fundamental and practical points of view. Several examples of core/shell type nanostructures are CdSe/CdS and CdS/CdSe, CdS/ZnS, CdSe/ZnS, CdS/HgS/CdS, ZnSe/CdSe, Si/SiO_2 [2-11].

The synthesis of core/shell CdSe/ZnS colloid nanocrystals is performed by pyrolysis method [10,11]. CdSe/ZnS QDs with diameters ranging from 23 to 55 Å are synthesized by pyrolysis of metal-organic compounds, such as dimethylcadmium (C_2H_6Cd) and trioctylphosphine selenide (TOPSe) in a coordinating solvent trioctylphosphine oxide (TOPO); oleic acid can be used as a stabilizer [11]. Diethylzinc ($ZnEt_2$) and bis(trimethylsilyl)sulfan ($(TMC)_2S$) are normally used as Zn and S precursors. In order to fabricate DiR nanostructures, directed shell growth is performed. CdSe QDs about 2-3 nm in diameter serve as seeds [11,15]. A schematic image of DiR nanostructure is shown on Figure 2.1.

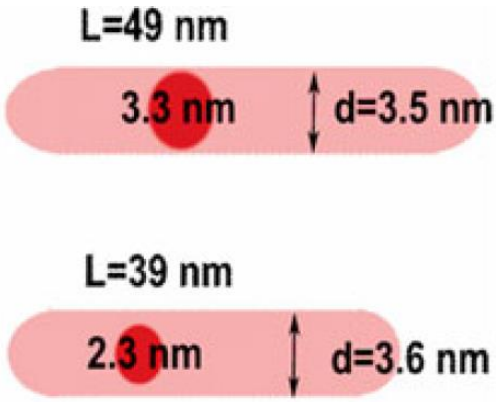

Figure 2.1. Schematic images of DiR core (red)/shell (pink) type nanostructures [11].

L – length; d – diameter.

2.2. Biological and medical applications of nanostructures

Nanostructures have attracted growing interest for various applications, such as chemistry, biochemistry, pharmacology and medicine [16]. In 1998, Bruchez and a group of researchers for the first time have reported application of quantum dots in immunofluorescence for labeling actin filaments in mice fibroblasts [17]. Later, quantum dots have been used for identifying a wide spectrum of proteins due to their ability to bind to specific antibodies [18-20]. A concept image of a quantum dot is shown on Figure 2.2. Hydrophobic drugs can be embedded into the structure between a hydrophobic nanoparticle core and a layer of amphiphile polymer; hydrophilic molecules can be immobilized on the nanostructure surface for specific binding to therapeutic compounds. From the moment of the first reported application of quantum dots for biological objects visualization in 2001, the nanostructures are actively used in in vivo and in vitro studies [4,21].

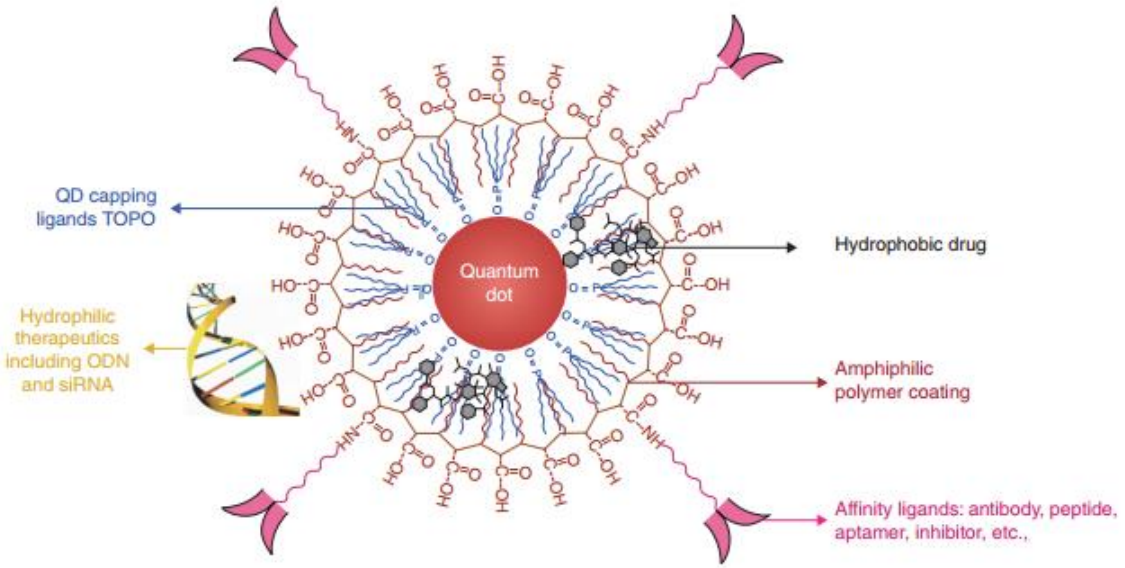

Figure 2.2. Schematic image of a multifunctional quantum dot covered by amphiphile polymer [20].

Lately much efforts have been put into reducing the potential toxicity of nanostructures by developing new compositions, new shells and fabricating smaller nanostructures in order to simplify cellular uptake for cells [22-25]. Bio-conjugation

ability, i.e. specific binding of nanostructures to antibodies antibodies that predominantly bind surface antigens in cancer cells; as well as creation of complexes of nanostructure with drugs, have induced research efforts dedicated to using them in diagnostics and treatment of oncological diseases [24].

2.2.1. Nanoparticles as fluorescent markers

Development of highly sensitive and specific probes that are more stable than organic dyes and fluorescent proteins is of great interest for many research areas, from molecular and cellular biology to molecular visualization and medical diagnostics [6,19,26] (Figure 2.3).

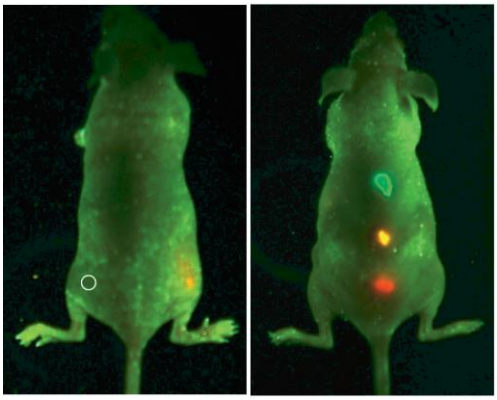

Figure 2.3. Bioluminescent images of living mice with injected nanostructures [21]. The left-hand image shows QD-tagged cancer cells, the right-hand image shows QD-encoded microbeads emitting green, yellow and red light.

Two strategies are used for incorporating nanostructures into cells: active method,– by using specific binding between nanocrystals and the surface of cancer cells, and passive approach targeting the nanostructures to the cells without specific binding [21].

2.2.2. Application of nanostructures in oncology

In 2004 a new class of quantum dot conjugates was developed. It possessed both hydrophilic and hydrophobic properties. It also contained an amphiphile triblock copolymer (composed of three polymer blocks) for *in vivo* protection, targeting ligands for recognition of cancerous tumor antigens and polyethylene glycol molecules (PEG) for improved biocompatibility and nanostructure circulation in the organism [21,27]. Antibodies conjugated to a QD are used for active tumor targeting, ensuring binding to a specific membrane agent [25].

In case of passive targeting, the macromolecules and nanoparticles accumulate in the tumor mostly due to enhanced permeation and retention [21]. It is believed that this effect arises from two factors:

- Tumor angiogenic vascular endothelial growth factors produce hyperpermeable blood vessels, leading to leakage of circulating macromolecules and small particles;
- Tumors lack an effective lymphatic drainage system, resulting in macromolecule or nanoparticle accumulation.

Apart from this, it is important to consider the processes responsible for nanostructure accumulation not only in tumors, but also in normal tissues as well. According to research performed by Xiaohu Gao group in 2004 [21], passive uptake of quantum dots and their retention happens mostly in livers and spleens, while is almost not observed in brains, hearts, kidneys or lungs.

2.2.3. Chiral nanostructures for biomedical applications

Investigations are ongoing on extending the capabilities of nanostructures by modifying their surface. Very recently the Balaz group [28] studied the induced circular

dichroism in CdSe quantum dots. The researchers discovered that chiral thiol ligands, such as L- and D-cysteine may induce chiral properties in initially achiral quantum dots.

For CdSe quantum dots capped by L- and D-cysteine a mirror image of signals in circular dichroism spectra is observed, as shown on Figure 2.4. In this case the origin of induced circular dichroism in quantum dots is explained by hybridization of chiral ligand molecular orbitals with the valence band of quantum dot [29].

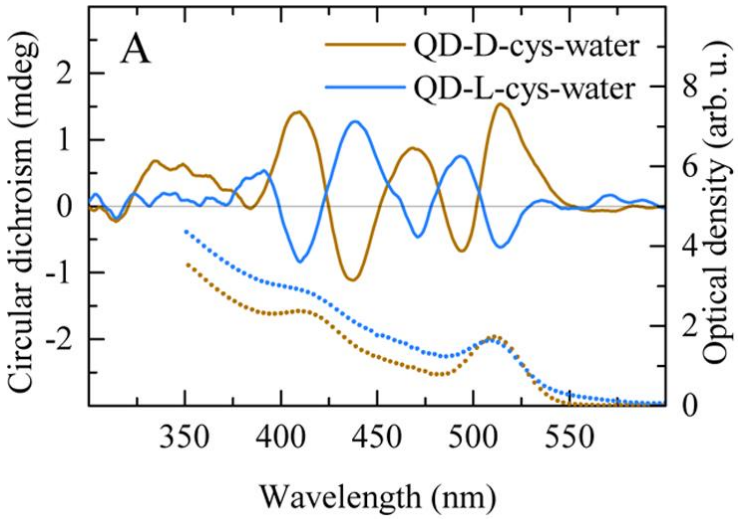

Figure 2.4. Spectra of induced circular dichroism (solid lines) of CdSe/ZnS quantum dots capped by L- and D-cysteine, dotted lines show absorption spectra [29]

Chiral quantum dots can be obtained by using chiral molecules as stabilizers in colloid synthesis or as ligands in post-synthesis phase transfer [30]. A theory was proposed that these chiral properties of quantum dots may affect their ability of interacting with biomolecules, and therefore modulate several vital processes in the living cells, because the most important elements of living organisms, the amino acids and nucleic acids, possess chiral properties.

Chiral compounds play a tremendous role in chemistry, pharmacology, biology and medicine. Chirality is also one of the key factors for molecular recognition, that has many applications in chemistry and biology [31-33]. It is known that stereoisomers are mirror images of each other and cannot be superposed. Development of effective methods for preparation and identification of pure enantiomeric compounds, composed

of stereoisomers is crucial for developing pharmaceutical drugs, agrochemicals, flavorings and food additives [34,35].

2.2.4 Using nanostructures in photodynamic therapy

Innovative technologies based on nanoparticles for fighting against oncological diseases and for improving already existing methods are currently being developed [36]. Photodynamic therapy (PDT) is one of the available cancer treatment methods, introduced into clinical practice about twenty years ago [36-38].

PDT effect is based on using compounds with photoallergic properties which selectively accumulated in malignant tumors. Typically used light radiation, mostly in the red spectral region, where the tissues are transparent for the light[39]. The aim of this method is to induce cytotoxic effect on the cancerous tumor. The basic principles of photodynamic therapy are shown in Figure 2.5. A photosensitizer with insignificant toxicity is injected into the organism (Figure 2.5A), subsequently accumulates mostly in cancerous cells which divide more quickly (Figure 2.5B). Then, the photosensitizer is activated by optical radiation (Figure 2.5C) and induces toxic effect on the cells, leading to their perish (Figure 2.5D).

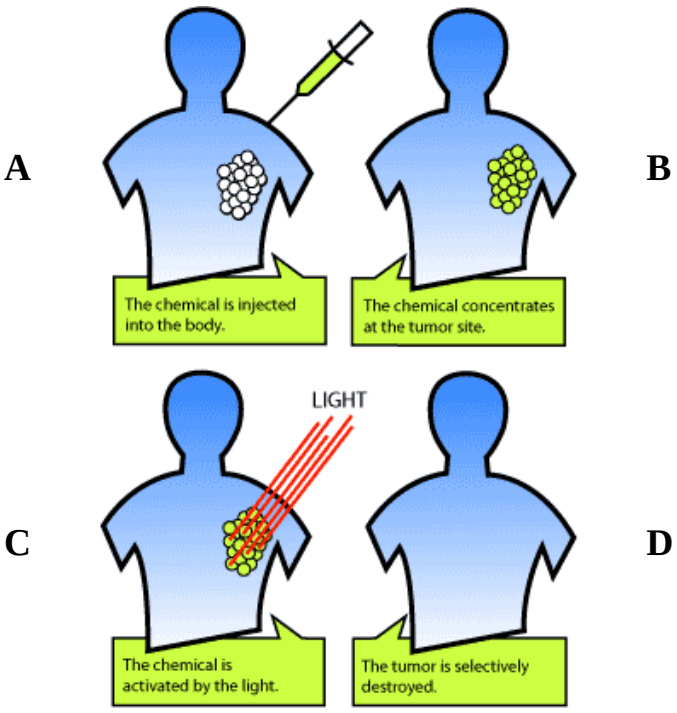

Figure 2.5. General principle of photodynamic therapy [40]

The Jablonski diagram explaining the photodynamic therapy process is shown in Figure 2.6. Upon illumination, the photosensitizer (PS) is excited from the ground state (S0) to the first excited singlet state (S1) with subsequent conversion to the triplet state (T1) [41] (Figure 1.6). The excited triplet state may react in two ways, defined as type I and type II mechanisms. The type I mechanism involves a reaction between a sensitizer in the excited state and a biological substrate, which yields free radicals and radical ions capable of causing irreparable damage to biological objects [42]. The type II mechanism results from the energy transfer between the sensitizer in an excited triplet state and molecular oxygen at the ground state, generating a singlet state of oxygen ($^1O_2$). This oxygen state can interact with a large number of biological cells, inducing oxidative damage and, ultimately, cell inactivation [42].

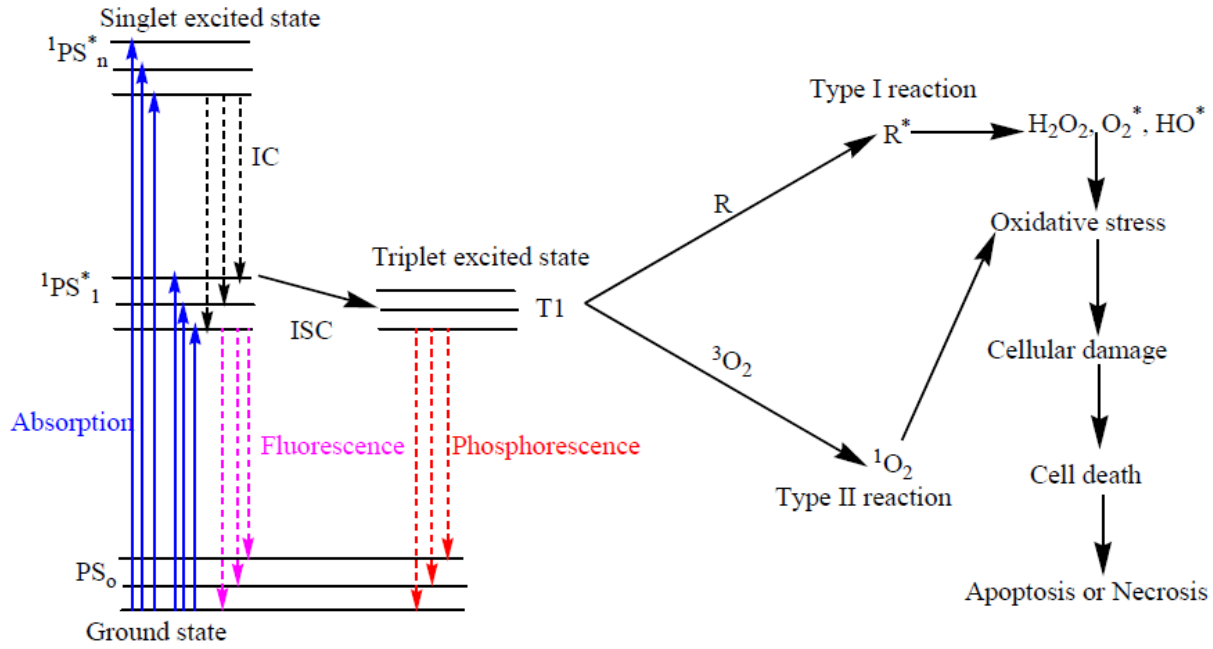

Figure 2.6. The modified Jablonski diagram explaining the photodynamic therapy process. Abbreviations: IC: internal crossing, ISC: intersystem crossing, PS: photosensitizer; 1PS*: excited singlet state; T1: triplet excited state; R: biological substrate;

R*: oxidized biological substrate; $^1O_2$: singlet oxygen state; H_2O_2: hydrogen peroxide; O_2^*: active form of oxygen; HO^*: hydroxyl radical [41].

Unique optical properties of quantum dots and their good stability led to an idea of using the quantum-dot/photosensitizer complexes for cancer photodynamic therapy in 2003 [43] (Figure 2.7).

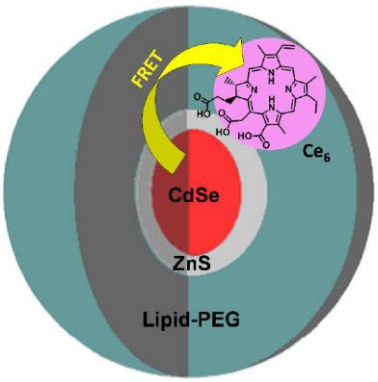

Figure 2.7. Quantum dot/chlorin e6 (Ce6) photosensitizer complex in a lipid shell [44].

Quantum dot/photosensitizer complexes can extend the photosensitizer excitation band and improve its efficiency. They may also solve the selectivity problem, therefore significantly increasing photosensitizer practicality. Quantum nanostructures in complexes with photosensitizers are suitable photoexcitation energy donors in the process of Förster resonance energy transfer (FRET), and can therefore increase the efficiency of molecular excitation [43].

2.3. Nanostructure–photosensitizer complexes

Nowadays many types of complexes of nanostructures and photosensitizer molecules for photodynamic therapy have been described [45,46,47], with their potential not yet fully uncovered. Several recent research publications demonstrated complexes where FRET processes can operate with energy transfer efficiency close to the value theoretically predicted [45]. However, photophysics of quantum dots sensitized by molecules is rather complex, thus unstudied and unexplained photoexcitation relaxation channels inside the complexes are observed. These processes lead to low intracomplex FRET efficiency [45-47].

2.3.1. Bonding mechanisms in complexes of nanocrystals and tetrapyrrole molecules

In order to obtain water-soluble complexes of quantum dots and photosensitizer molecules, solubilization of nanostructures with hydrophillic ligands is usually performed. Covalent bonding has been demonstrated to make complexes of nanocrystals and tetrapyrrole molecures. It typically include two steps. Firstly, hydrophobic nanostructures CdSe/ZnS/TOPO are bound with cysteine. On the second stage the cysteine molecules are substituted for molecules with hydroxylic end-groups of polyethylene glycol (PEG-OH) thiol and amino end-groups of polyethylene glycol

(PEG-NH_2) thiol [47]. It allows creating stable colloid solutions of quantum dots. 1-Ethyl-3-(3- dimethylaminopropyl)carbodiimide (EDAC) is used as a linking agent.

An example of obtaining complexes formed by electrostatic interaction is variants with hydrophobic CdSe/ZnS/TOPO nanoparticles solubilized by 2-(dimethylamino)ethanthiol (DMAET) molecules in order to provide a positive charge on the surface of QDs [47].

A water-soluble metal-free tetra(p-trimethylamino)phenyporphyrin (TAP), which is a positively charged product of tetraphenylporphyrin, is used as a photosensitizer; another photosensitizer example is chlorin e6 [49].

2.3.2. Photophysical properties of nanostructure-containing complexes

In nanostructure complexes with tetrapyrrole molecules an alteration of the tetrapyrrole molecule spectral form compared to its free state is often observed [47].

TAP absorption spectra plotted as the difference between the spectra of complexes and unbound nanostructures are shown on Figure 2.8. When TAP interacts with the nanostructures, the peak of its band is shifted into the red spectral region.

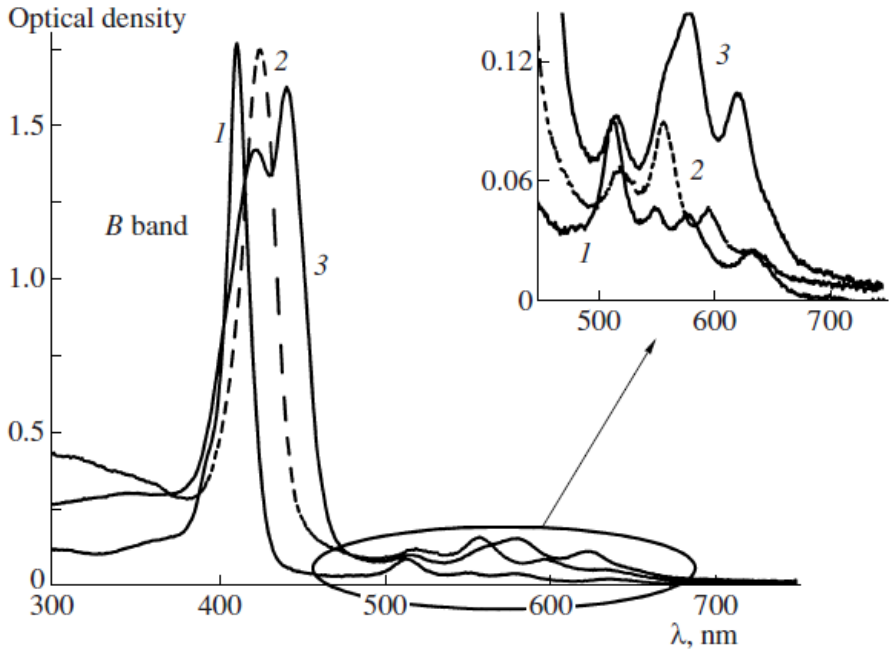

Figure 2.8. Absorption spectra (1) of free TAP, (2) TAP in the presence of quantum dots with 2.75 nm diameter in the solution, and (3) TAP in the presence of quantum dots with 3 nm diameter [47]

Similarly, after adding chlorin e6 to the nanostructure solution in distilled water a significant change in chlorin e6 absorption spectrum is observed, as seen from Figure 2.9. Therefore, a shift of the first absorption band and an appearance of a second absorption band around 500 nm are observed. The Soret band remains almost unmoved, but its significant broadening is observed.

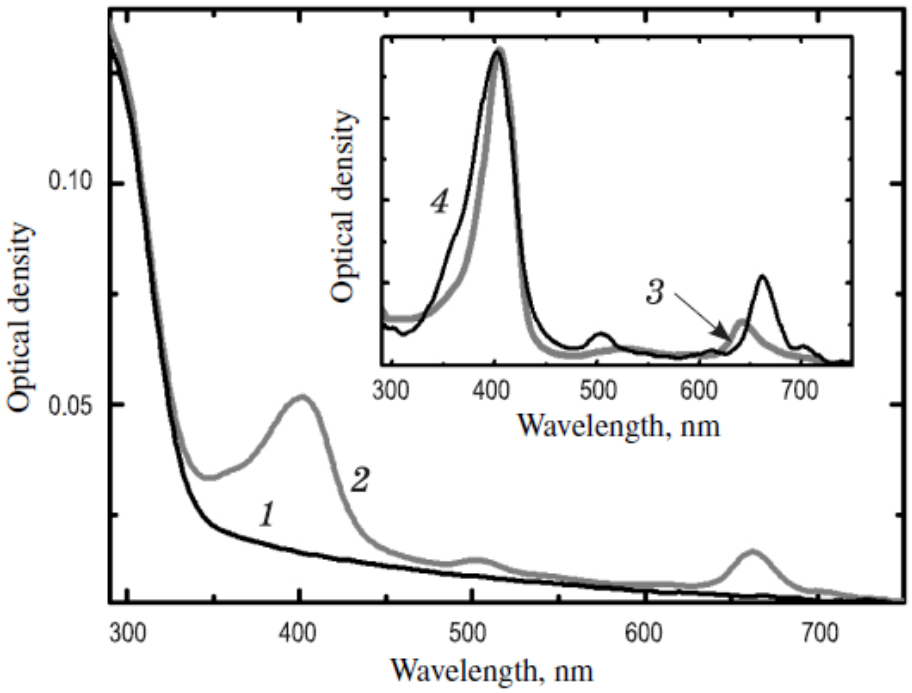

Figure 2.9. Absorption spectra. 1 - QD, 2 - QD-chlorin e6 complexes. Differential absorption spectrum of free chlorin e6 and its absorption spectrum in a QD-complex are shown on the inset (curves 3 and 4 respectively) [48]

It is noted that adding photosensitizer into the nanostructure solution leads to a decrease in nanostructure luminescence intensity as well as to appearance of a luminescent band of the photosensitizer associated in a complex with the nanostructures [48]. This process is depicted on Figure 2.10.

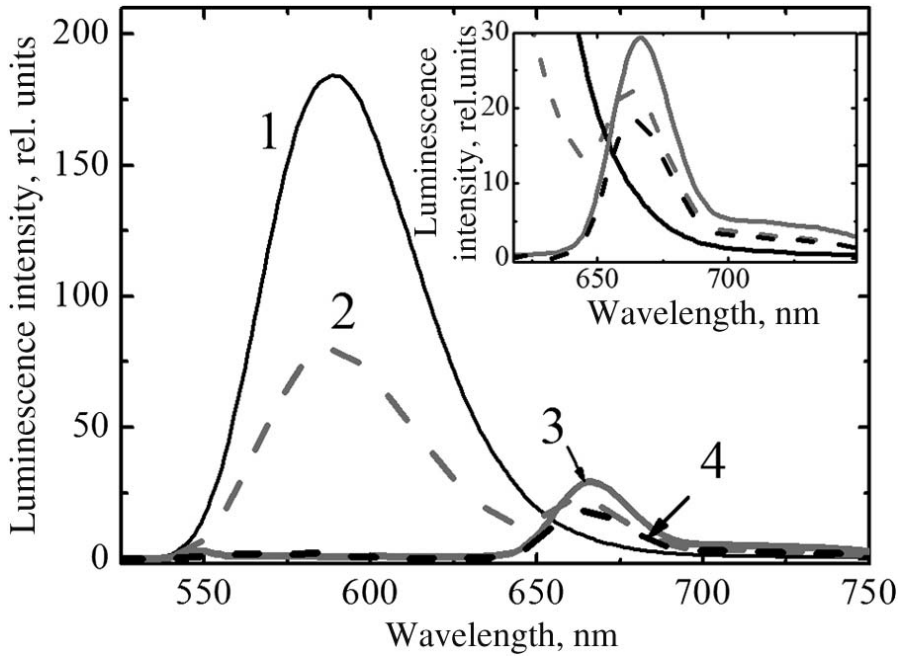

Figure 2.10. Luminescence spectra. 1 and 2 – ZnS: Mn before and after mixing the QD solution with a solution of Ce6 (excited by 300 nm radiation); 3 – QD/Ce6 mixed solution (excited by light with wavelength 400 nm); 4 – luminescence spectrum of Ce6, obtained as a result of subtracting the luminescence spectrum of QDs from the luminescence spectrum of the mixed QD/Ce6 solution (2). The inset shows 615–740 nm section of the spectrum at an enlarged scale [48].

Luminescence quenching in nanostructures as a result of their association in a complex with tetrapyrrole or similar molecules is considered to be one of the most characteristic behaviors during complexation. Some research results show how the chiral properties of chlorin e6 are changing in the process of binding into complex with semiconductor nanostructures [50].

2.4 Conclusions

Based on the performed analytical review, the following conclusions can be made:

- A thorough approach to study photophysical properties of nanocrystals with different modifications and complexes based on them is required for successful applications of semiconductor nanostructures in different fields, including medicine.
- The chirality of nanocrystals plays a tremendous role in the living objects, and thus it should be considered in the processes of fabricating hybrid nanostructures designed for studying biological samples.
- Semiconductor nanocrystals are suitable photoexcitation energy donors in the FRET process in nanostructure/photosensitizer complexes, therefore allowing to improve the PDT efficiency.

In this work we studied optical and photophysical properties of chiral nanocrystals, performed research of induced nanostructure chirality influence on their cellular absorption in the living cells of Ehrlich ascites carcinoma, and investigated chiral nanocrystals interaction with chlorin e6.

3 Research methods and materials

3.1. Reagents

We used chloroform as a solvent for hydrophobic nanoparticle fabrication: CdSe/ZnS QDs and CdSe/CdS DiRs. Methanol was used for nanostructure purification. The nanostructures were solubilized by hydrophilic L- and D-cysteine molecules, dissolved in methanol with addition of hydrochloric acid.

We used DMEM (Dulbecco's Modified Eagle Medium) for testing nanostructure stability in biological media. DMEM is a sterilized mixture of non-organic salts, amino acids, vitamins, glucose and phenol red in purified water.

Distilled water and dimethyl sulfoxide (DMSO) are served as solvents for hydrophilic nanostructures and complexes based on them.

The reagents were purchased from Aldrich and used without preliminary purification.

Optically active levorotatory chlorin e6 purchased from Fronter Scientific, that did not require further purification, was used as a photosensitizer.

3.2. Materials

In this work we used semiconductor CdSe/ZnS core/shell quantum dots with a luminescence band peak centered at 530 and 580 nm, hereinafter for brevity, referred to as 530 QDs and 580 QDs. Another type of nanostructures used was CdSe/CdS quantum dots in quantum rods synthesized using methods shown in Ref. 11 and 14 with a luminescence band maximum at 620 nm, hereinafter for brevity, referred to as 620 DiRs.

3.3 Equipment and methods for nanostructure characterization

IR spectra of the samples were recorded for providing evidence of successful solubilization of nanostructures by L- and D-cysteine. A Fourier transform infrared (FTIR) spectrometer Tensor 27 (Bruker), designed for scanning in 4000–400 cm^{-1} range, was used for performing the analysis.

Chirality of nanostructures was investigated using a circular dichroism spectrometer JASCO J-1500 (JASCO analytical instruments), designed for studying circular dichroism in a spectral range of 300-700 nm.

The forms, sizes and size dispersions of the nanostructures were estimated using a scanning electron microscope (MERLIN. Carl Zeiss) with Oxford Instruments Nanoanalysis tools.

Nanostructures and their complexes with chlorin e6 were studied by stationary optical spectroscopy methods. The absorption and fluorescence spectra were recorded using a UV-3600 spectrophotometer (Shimadzu) and a Cary Eclipse spectrofluorimeter (Varian), respectively.

We used laser scanning luminescent microscope MicroTime 100 (PicoQuant) for measuring luminescence decay times. In this work luminescence decay of nanostructures was recorded using optical bandpass filters transparent in 580, 620 and 670 nm regions for registering luminescence of QDs, DiRs and chlorin e6, respectively.

In order to acquire luminescent images of nanostructures in cancerous cells, we used a laser scanning confocal microscope LSM 710 (Carl Zeiss) that is designed for operation in visible spectrum and allows spectral and sectional analysis of the samples.

The sizes of quantum dots were defined using an empirical equation for CdSe compounds [12]

$$d_{CdSe} = (1.6122 \cdot 10^{-9})\lambda^4 - (2.6575 \cdot 10^{-6})\lambda^3 + (1.6242 \cdot 10^{-3})\lambda^2 - (0.4277)\lambda + 41.57, \quad (3.1)$$

where d_{CdSe} is the nanostructure core diameter, and λ is the wavelength corresponding to a position of exciton absorption band of the quantum dot.

The thickness of ZnS shell is considered to be 5 Å [12,13].

The extinction coefficient was calculated as follows

$$\varepsilon = 5857 \cdot (d)^{2.65}, \quad (3.2)$$

where ε is the extinction coefficient ($M^{-1}cm^{-1}$), and d is the size of nanocrystals (nm).

For calculating the DiR parameters we used an empirical equation for CdS compounds

$$d_{CdS} = (-6{,}6521 \cdot 10^{-8})\lambda^3 + (1{,}9557 \cdot 10^{-4})\lambda^2 - (9{,}2352 \cdot 10^{-2})\lambda + 13{,}29 \quad (3.3)$$

Here, the extinction coefficient is defined as

$$\varepsilon = 21536 \cdot (d)^{2,3} \quad (3.4)$$

The core diameters of CdSe QDs and DiRs were approximately 3,5 and 4 nm, respectively. The length of a rod-shaped shell in the CdS DiRs was about 6 nm.

Optical parameters of nanocrystals include absorption and photoluminescence spectra, as well as luminescence quantum yield and its decay kinetics.

Luminescence quantum yield (φ) is calculated as a ratio between the numbers of emitted (N_{emit}) and absorbed quanta (N_{abs})

$$\phi = \frac{N_{emit}}{N_{abs}} \quad (3.5)$$

Luminescence quantum yield of nanostructures is usually defined by comparative method that requires using a sample with the known value of luminescence quantum yield as a reference. Most often, rhodamine 6G with quantum yield 95% is used as

reference. Therefore, the following equation is used for defining the luminescence quantum yield of nanostructures

$$\varphi = \varphi_0 \cdot \frac{\int I_{sam} d\lambda \cdot n_{sam}^2 \cdot D_{ref}}{\int I_{ref} d\lambda \cdot n_{ref}^2 \cdot D_{sam}}, \quad (3.6)$$

where φ_0 is luminescence quantum yield of the reference, $\int I_{sam} d\lambda$, $\int I_{ref} d\lambda$ are integral luminescence quantum yields of the sample and the reference, respectively, D_{sam}, D_{ref} are optical densities of the sample and the reference at the luminescence excitation wavelength, n_{sam}, n_{ref} are refractive indices of the sample and reference solvents.

Luminescence lifetime of nanostructures fits well into a multiexponential decay model:

$$\mathrm{I(t)} = y_{0n} + \sum_n \left(A_n \exp\left(-\frac{t}{\tau_n} \right) \right), \quad (3.7)$$

where A_n and τ_n are fluorescence amplitudes and lifetimes of nanostructures.

Mean luminescence lifetime was calculated using the following equation

$$\langle \tau \rangle = \frac{\sum_n A_n \cdot \tau_n^2}{\sum_n A_n \cdot \tau_n} \quad (3.8)$$

Nanostructure preparation

Preliminary purification of samples was performed for removing the excessive stabilizer molecules and impurities:

5 mg of solid nanostructures were dissolved in 500 μl of chloroform, then 1 ml of methanol was added to the solution; and then it was intensely stirred and precipitated in a centrifuge (1 min, 15 000 rpm). The procedure was repeated 2-3 times for each sample.

We used the following solubilization procedure for chiral nanostructure fabrication:

Precipitated nanostructures are dissolved in 750 μl of chloroform. The nanostructure solution in chloroform is kept at -20 °C for 15 min, and after that 37,5 μl of L-,D-cysteine solution in methanol is added until the formation of flakes in the nanostructure solution. The mixture is intensely shaken, 1 ml of water and 90 μl of concentrated KOH solution are added. The mixture is shaken again, until approximately a half of the nanostructures transfers to the aqueous phase. The fabricated aqueous solution of nanostructures is used for further analysis.

The following method was used for preparing cysteine solution in methanol:

25 mg of cysteine are dissolved in a mixed solution of methanol and hydrochloric acid. After complete cysteine dissolution in methanol, a concentrated solution of potassium hydroxide is added for neutralizing the acid.

In case of 530 QD CdSe/ZnS solubilization, a L- and D-cysteine hydrochloride solution in methanol (2 mol/l) was added to a chloroform solution of CdSe/ZnS /TOPO ($C_{QD} \sim 5 \cdot 10^{-5}$ mol/l). The volume of the added solution did not exceed 10% of the initial volume of QD solution. The reaction mixture was shaken for 1 min, after that water was added. The pH value was increased to 10 by adding NaOH solution. The solubilized nanostructures were then transferred to the aqueous phase. The fabricated aqueous solution of chiral nanostructures was used for further analysis.

Introducing the nanostructures into EAC cells

The Ehrlich ascites carcinoma (EAC) cell culture was obtained from the Petrov Research Institute of Oncology from white laboratory mice with an average weight of 20 g after 8-9 days of ascite growth.

The EAC cells were incubated with quantum dots in a well plate at 37 °C in a humidified 5% CO_2 atmosphere for 3, 6, 24, 48 and 96 h in RPMI-1640 medium containing 10% of bovine embryonic serum and 100 U/ml of penicillin. The cell concentration was 4×10^6 cells per well.

After incubation the cells were washed 3 times and suspended in HBSS. The images of living cells were recorded by LSM 710 (Zeiss) laser scanning confocal microscope equipped with a x20/0.4 NA objective.

Formation of nanostructure complexes with photosensitizer molecules

In this work we performed a study of formation conditions, stability and photophysical properties of chiral nanostructure complexes formed in DMSO by DiRs and chlorin e6 (Ce6) molecules. Samples with ratios of photosensitizer concentration to nanostructure concentration (*n*) 1:1, 2:1, 3:1, 15:1, 50:1, 100:1 were fabricated. For studying the influence of Ce6 concentration on spectral properties of the obtained nanostructure/Ce6 complexes, microscopic amounts of Ce6 solution were gradually added to the nanostructure solution.

4 Optical properties of chiral semiconductor nanocrystals

In this chapter we discuss the optical properties of two nanocrystal types: CdSe/ZnS quantum dots (QDs) of different sizes and CdSe/CdS quantum dots in quantum rods (DiRs), as well as the influence of solubilization procedure using L- and D-cysteine enantiomers on their spectral luminescent properties.

4.1. Spectral luminescent properties of hydrophobic NCs

Prior to solubilization process, investigation of spectral luminescent properties was conducted. Absorption and luminescence spectra of 580 CdSe/ZnS QDs in chloroform are shown on Figure 4.1.

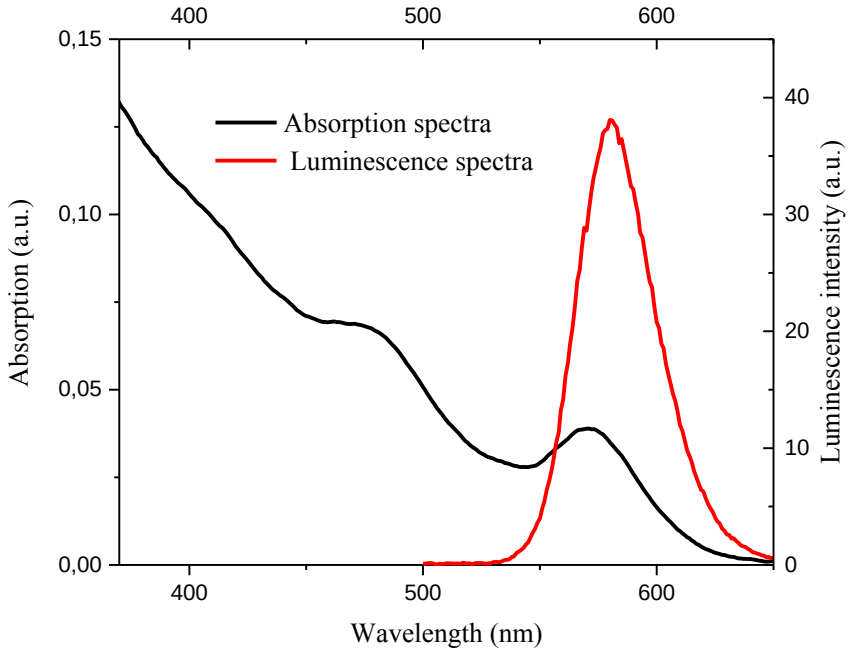

Figure 4.1. Absorption and luminescence spectra of 580 QDs in chloroform. Luminescence was excited with 450 nm light source.

Based on the observed spectral luminescent properties, it can be seen that the 570 nm peak corresponds to a position of the first exciton absorption band of this quantum

dot ensemble. The maximum of nanocrystal luminescence is centered at 580 nm. The luminescence spectrum does not include any additional bands, therefore the luminescence origin may be attributed to exciton.

For defining luminescence decay times of 580 QDs, we registered the decay curves using a luminescent microscope MicroTime 100 with a bandpass filter. Its maximum transmission was centered at 580 nm with 10 nm FWHM. Figure 4.2 shows the luminescence decay curve of 580 QDs.

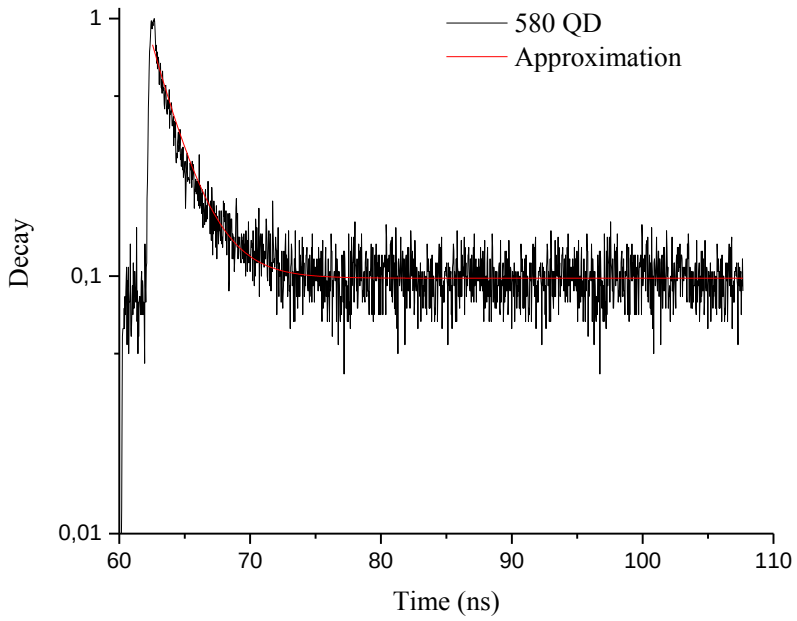

Figure 4.2. Luminescence decay curve for colloid solution of 580 QDs in chloroform

We used two-exponential dependence for approximation; mean luminescence decay time for QDs was calculated using Equation 3.8, for 580 QDs it was about 10.46 ns (Table 4.1).

Absorption and luminescence spectra were measured for DiRs in the same way. The acquired data is presented on Figure 4.3.

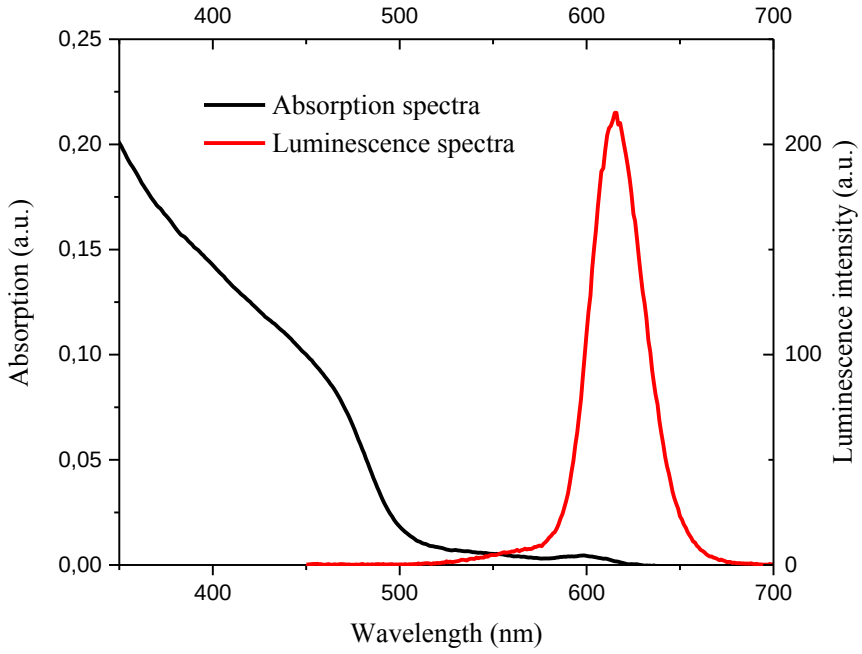

Figure 4.3. Absorption and luminescence spectra of 620 DiRs in chloroform. Luminescence was excited with 450 nm light source.

Spectral-luminescent analysis data demonstrates that the 600 nm band corresponds to CdSe exciton absorption band, and 460 nm peak corresponds to the CdS band. The maximum of nanostructure luminescence was positioned at 620 nm. No additional bands were observed in the luminescence spectrum, therefore luminescence in 620 DiRs can be of exciton origin, too.

Luminescence decay was registered using an interference filter centered at 620 nm (Figure 4.4).

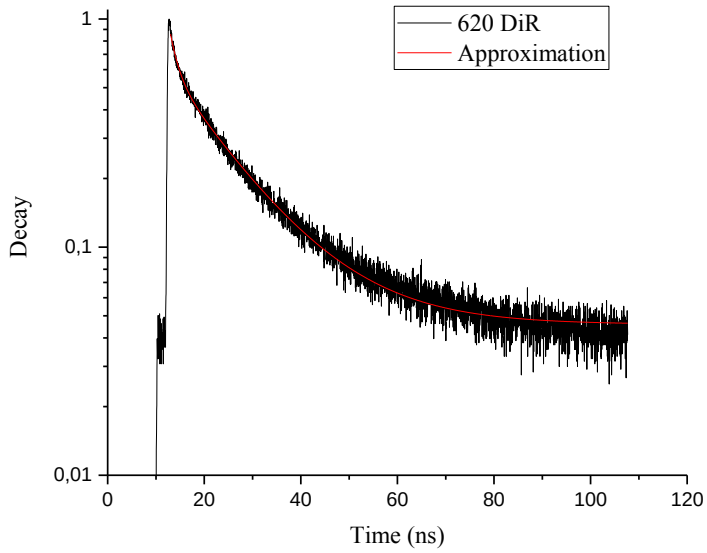

Figure 4.4. Luminescence decay curve of 620 DiRs in chloroform.

We used two-exponential dependence (Equation 3.7) for approximation. Mean luminescence lifetime (Equation 3.8) for hydrophobic 620 DiRs was found to be 9 ns (Table 4.1).

Absorption and luminescence spectra for 530 QDs were measured using the same technique. The acquired data is presented on Figure 4.5.

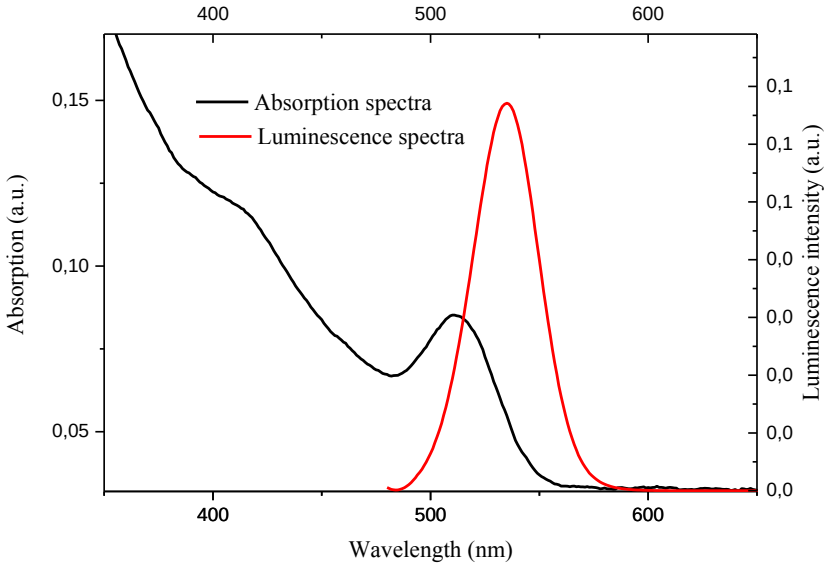

Figure 4.5. Absorption and luminescence spectra of 530 QDs in chloroform. Luminescence was excited with 450 nm light source.

Based on the observed spectral luminescent properties, one may see that the 570 nm peak corresponds to a position of the first exciton absorption band of the quantum dot. The maximum of nanostructure luminescence is positioned at 530 nm. Luminescence decay was registered using an interference filter centered at 530 nm. Luminescence quenching curve is shown of Figure 4.6.

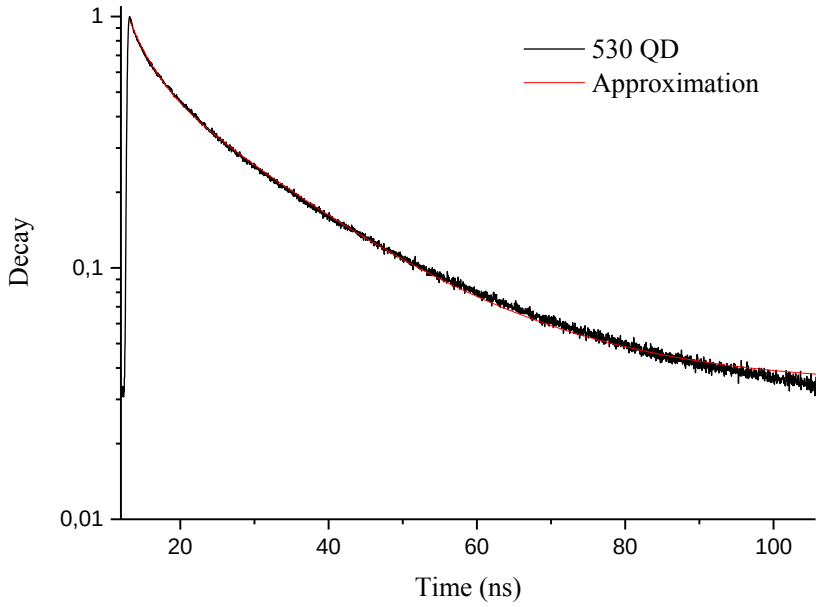

Figure 4.6. Luminescence decay curve of 530 QDs in chloroform.

We used two-exponential dependence (Equation 3.7) for approximation. Mean luminescence decay time (Equation 3.8) for 530 QDs was found to be 18 ns (Table 4.1).

Table 4.1. Spectral luminescent parameters of various hydrophobic nanostructures

NC	Luminescence quantum yield, %	Amplitude A_1, %	τ_1, ns	Amplitude A_2, %	τ_2, ns	$<\tau>$, ns
580 QD	1.5	50±10	1.8	50±10	11.74	10.46
620 DiR	3.9	86±2	4.4	14±2	16.33	9.03
530 QD	11.6	95±1	2.9	5±1	18.22	18.0

4.2. FTIR characterization of nanostructures

For fabricating nanostructures with induced chirality we used phase transfer method from organic phase into aqueous, with the help of cysteine enantiomers, as described in Chapter 3.

In order to prove successful solubilization of nanostructures with L- and D-cysteine, infrared (IR) spectra of the nanostructures were registered. Figure 4.7 shows the IR spectra of capped 580 QDs, 620 DiRs and 530 QDs.

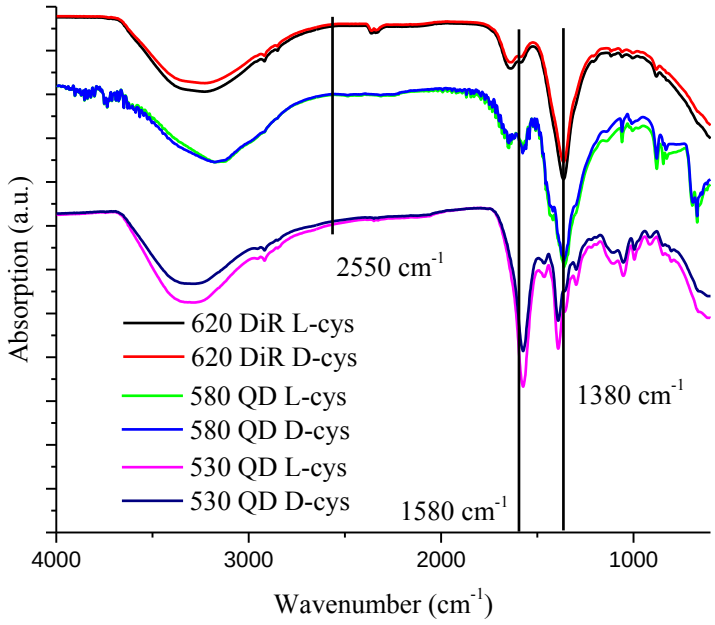

Figure 4.7. Infrared absorption spectra of chiral nanostructures capped with L- and D-cysteine

According to studies [51] and [52], the presence of two peaks in the region around 1380 cm^{-1} and 1580 cm^{-1}, corresponding to the symmetric stretching vibration of the carbonyl COO^- group and the asymmetric bending vibration of the $NH3_+$ group, respectively, confirms that these groups in cysteine molecules are free. Absence of the peak at 2550 cm^{-1} related to a thiol group –SH [53], indicates successful binding of cysteine with the nanostructure surface through this group.

4.3. Electron microscopy characterization of nanostructures

In order to get information about the forms, mean sizes and size dispersion of the chiral nanocrystals capped with L- and D-cysteine, the samples were investigated using electron microscopy methods. SEM images of 580 QD and 620 DiR nanostructures are shown on Figures 4.8 and 4.9.

During phase transfer process there is a large probability of spontaneous merging, i.e. aggregation of nanostructures, therefore electron microscopy was used for controlling the condition of chiral NC aggregates as well.

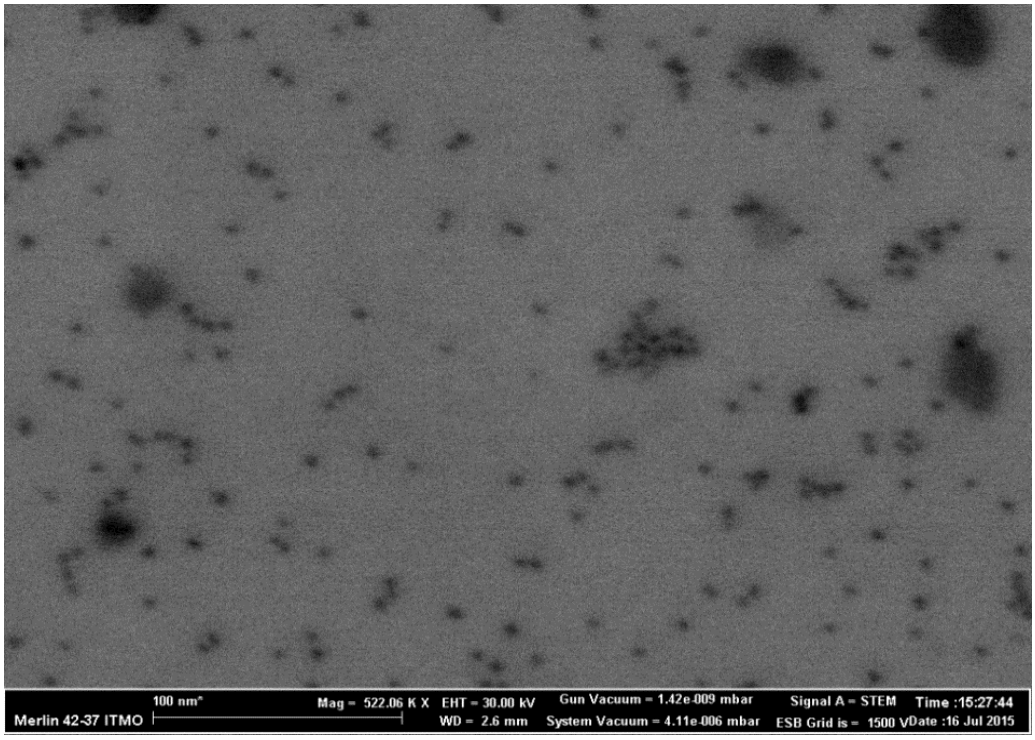

Figure 4.8. SEM image of 580 QDs

No visible nanocrystal size dispersion is observed on Figure 4.8, and the sizes (3-4 nm in diameter) mostly correspond to estimations calculated from the position of the exciton absorption band using an empirical Equation 3.1 from Ref. 12.

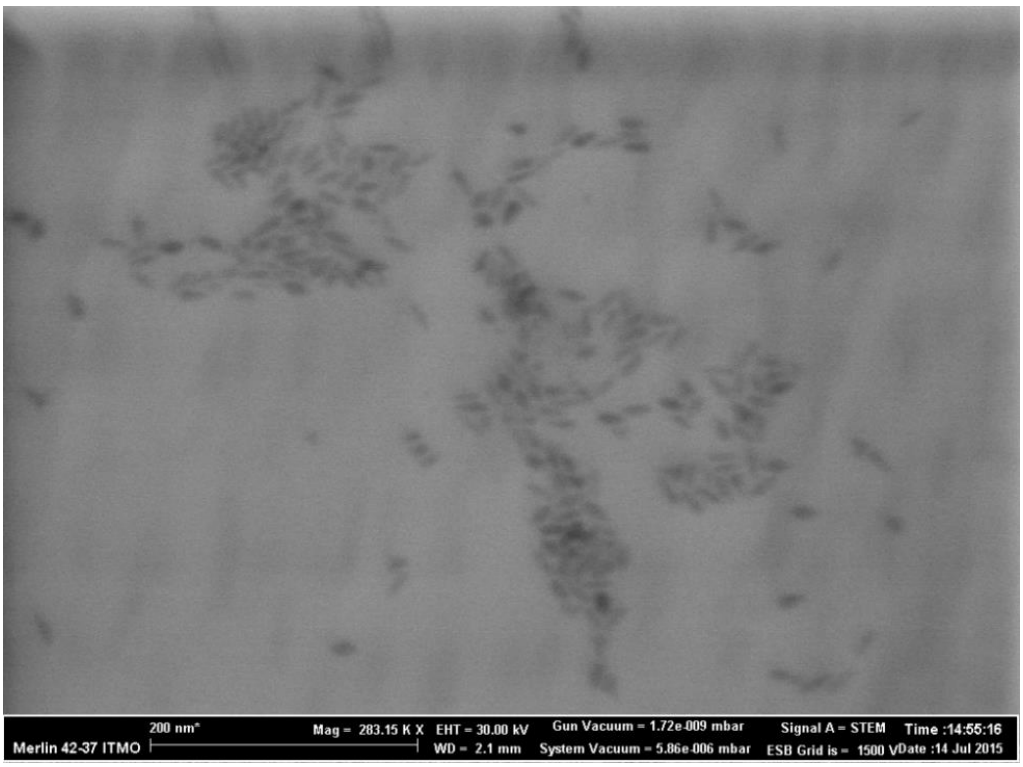

Figure 4.9. SEM images of 620 DiRs

Mean parameters of DiR nanostructures are 10 nm in length and 4 nm in diameter, which is in agreement with the size estimations from empirical Equations 3.1 and 3.3. No aggregation is observed in nanostructure samples capped with cysteine enantiomers.

4.4. Optical properties of chiral NCs

Solubilization of nanocrystal surface by enantiomers of chiral molecules may result in inducing chirality of the former, which in turn leads to an appearance of several peaks in their circular dichroism spectra, corresponding to electron transition bands of nanostructures. Because of unequal absorption of light with different circular polarizations, it is necessary to measure circular dichroism spectra of L- and D-cysteine capped 580 QDs, 620 DiRs and 530 QDs. Circular dichroism spectra that were recorded simultaneously with the absorption spectra are presented on Figures 4.10, 4.11 and 4.12.

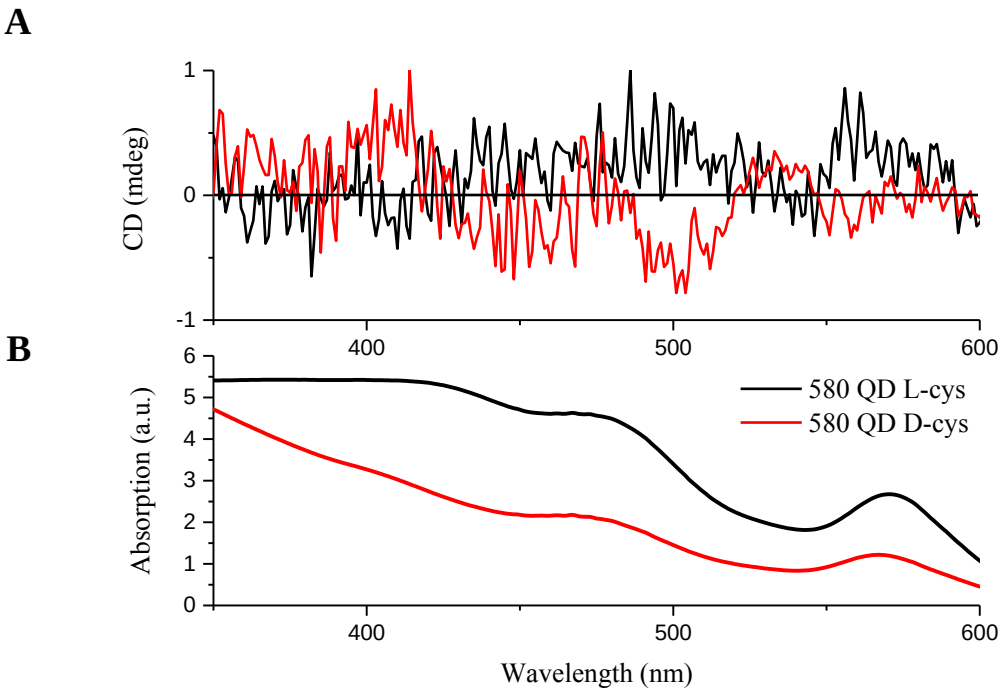

Figure 4.10. Circular dichroism (A) and absorption (B) spectra of 580 L- and D-cysteine capped QD colloid solution

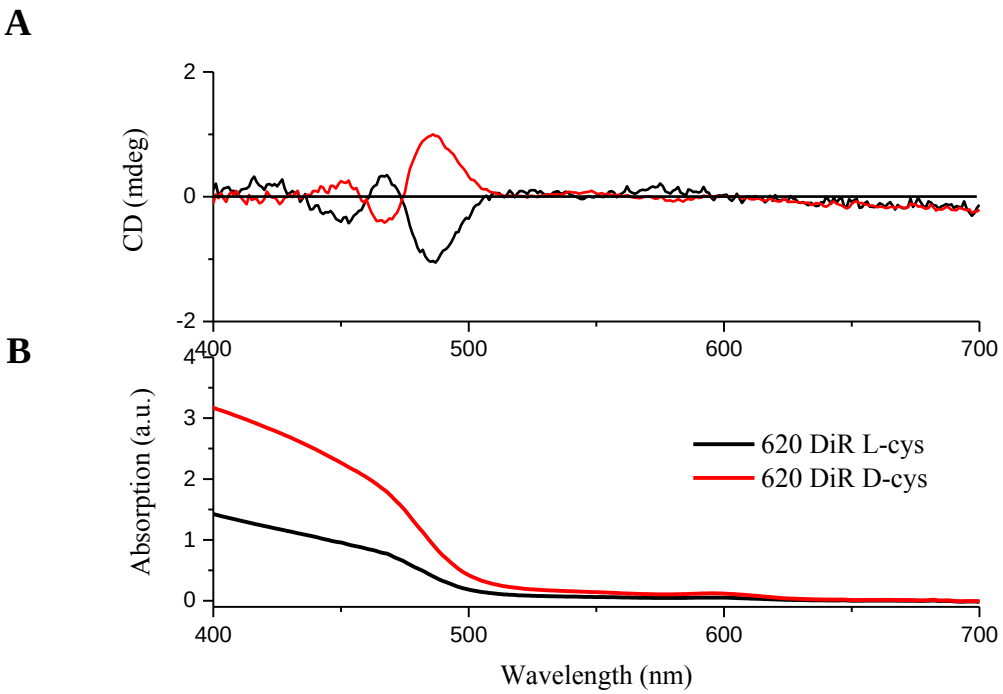

Figure 4.11. Circular dichroism (A) and absorption (B) spectra of 620 L- and D-cysteine capped DiR colloid solution

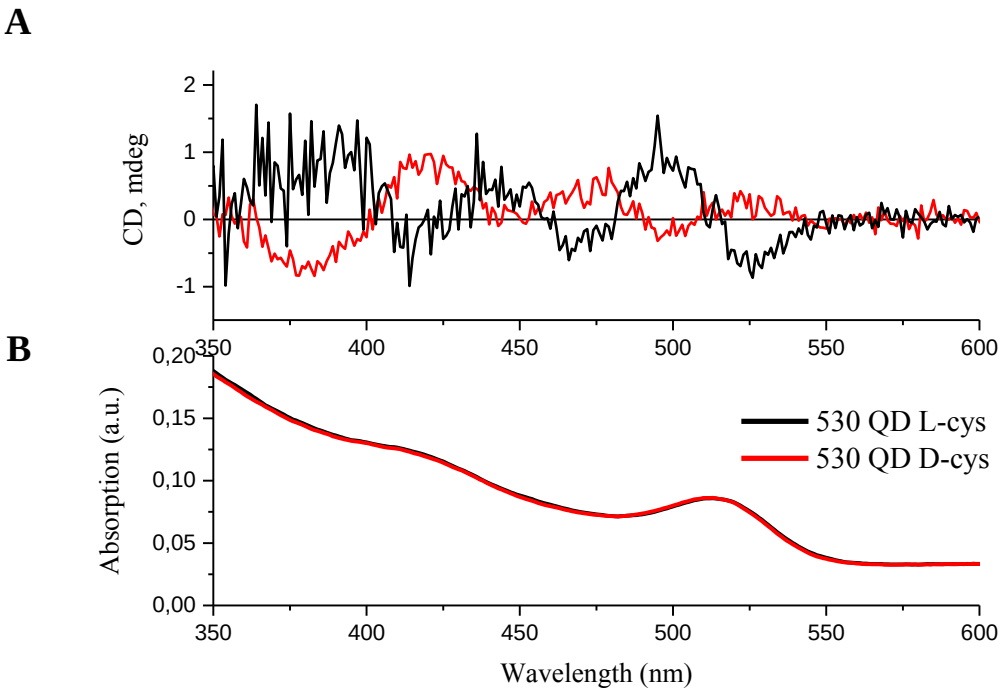

Figure 4.12. Circular dichroism (A) and absorption (B) spectra of 530 L- and D-cysteine capped QD colloid solution

Absorption spectrum analysis of hydrophilic nanocrystals has shown that for all types of nanostructures phase transfer from the organic to the aqueous phase in the presence of L- and D-enantiomers does not lead to any significant changes in their absorption spectra.

As can be seen from Figures 4.10-4.12, the peaks situated at NC electron absorption bands, which have amplitudes with opposite signs for L- and D-enantiomers, appeared in CD spectra of all structures. Signal symmetry in the areas of circular dichroism spectra corresponding to exciton absorption bears evidence of successful solubilization of nanostructures with chiral ligands [29].

After NC solubilization the luminescence spectra of nanostructures were measured, shown on Figures 4.13-4.15. Luminescence was excited with a 450 nm light source.

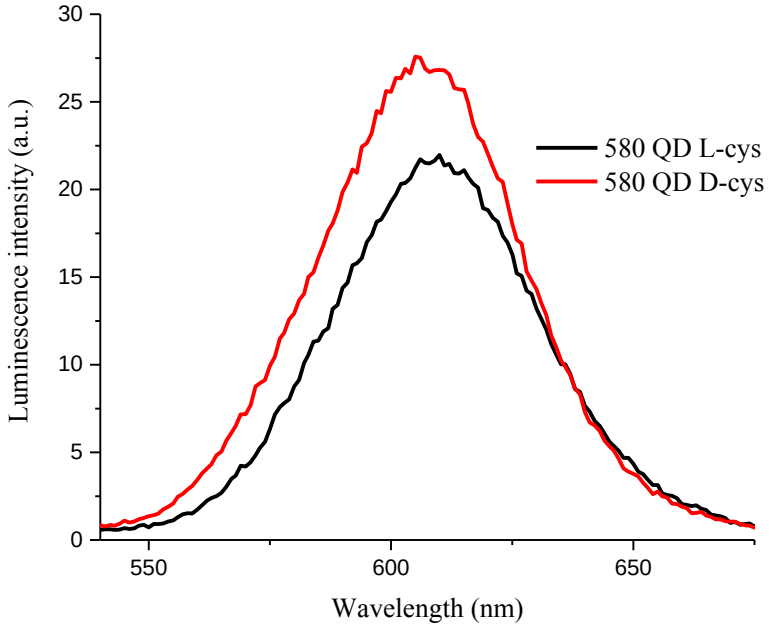

Figure 4.13. Luminescence spectra of L- and D-cysteine capped 580 QDs excited by 450 nm radiation

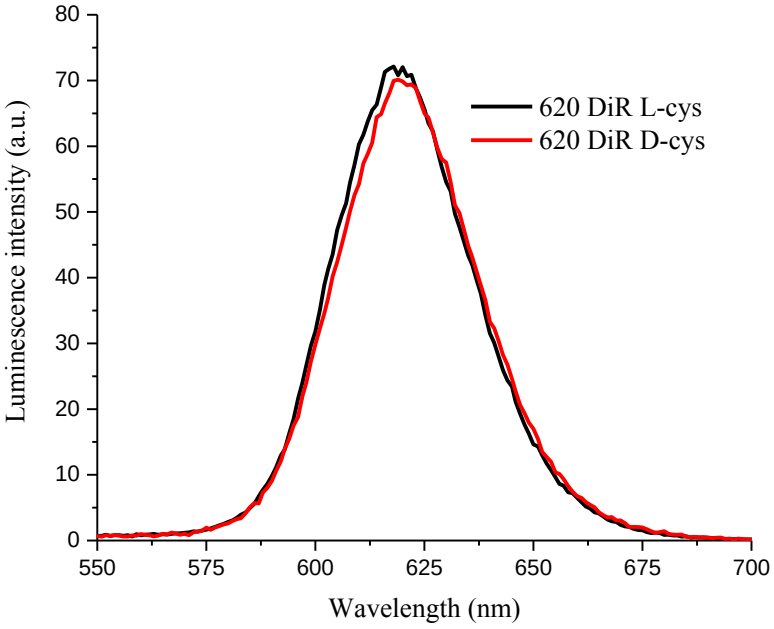

Figure 4.14. Luminescence spectra of L- and D-cysteine capped 620 DiRs excited by 450 nm radiation

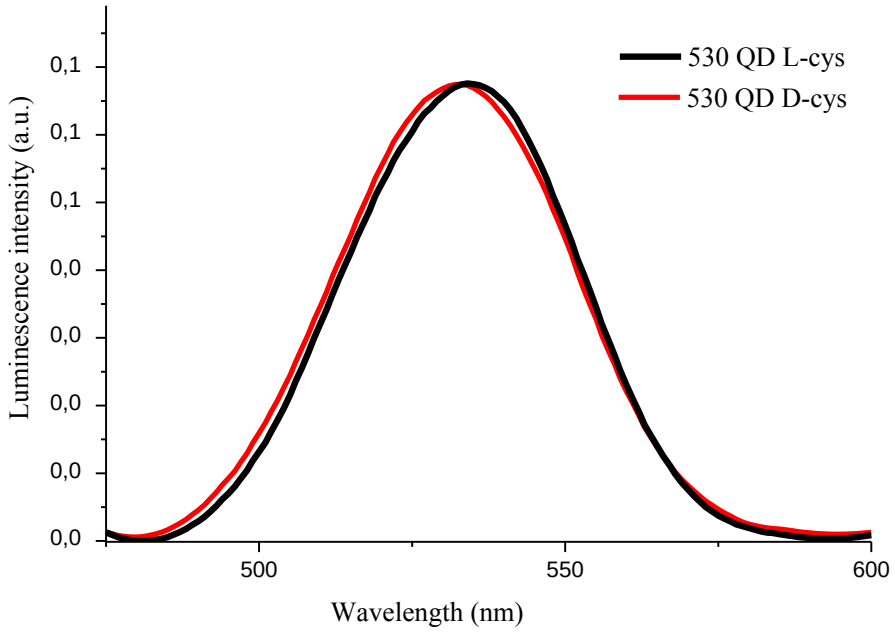

Figure 4.15. Luminescence spectra of L- and D-cysteine capped 530 QDs excited by 450 nm radiation

Analysis of spectral luminescent properties of hydrophilic NCs demonstrated that for all types of nanostructures a decrease of luminescence quantum yield compared to the hydrophobic nanostructures is observed. Quantum yield values for all types of chiral structures are given in Table 4.2.

We also studied luminescence kinetics of the chiral nanostructures, as presented in Figure 4.16, 4.17 and 4.18.

A **B**

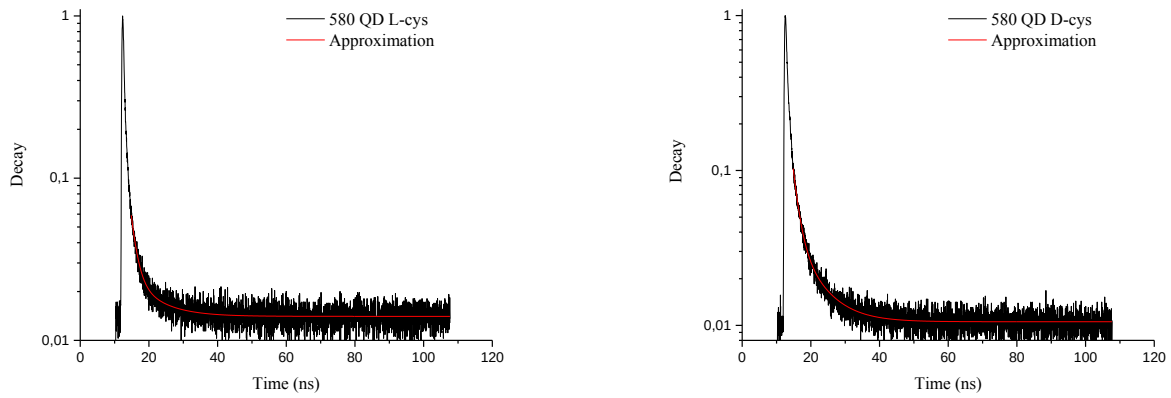

Figure 4.16. Luminescence decay curves for L- (A) and D-cysteine capped 580 QDs in water

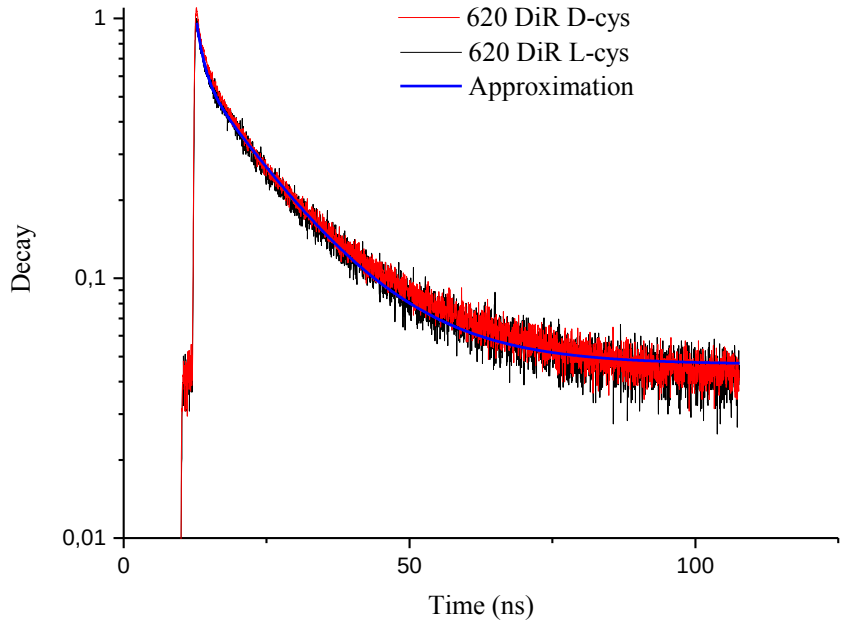

Figure 4.17. Luminescence decay curves for L- and D-cysteine capped 620 DiRs in water

A **B**

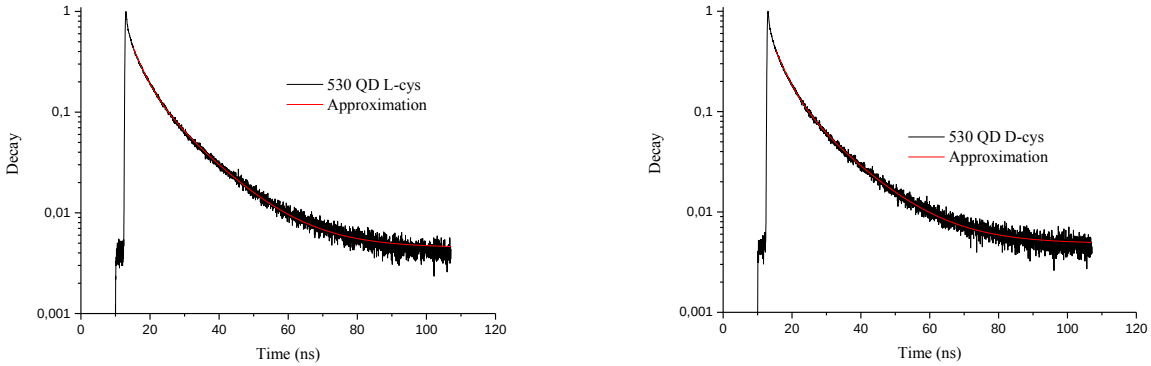

Figure 4.18 Luminescence decay curves for L- (A) and D-cysteine (B) capped 530 QDs in water

The analysis of nanostructure luminescence decay curves has revealed a reduction in luminescence decay times for all types of nanostructures, which correlates with their decrease of luminescence quantum yields. Luminescence decay time of 580 QDs significantly decreased to 2.16 and 2.25 ns, respectively, after solubilization with L- and D-cysteine. In 620 DiRs luminescence decay time decreased to 1.6 ns after solubilization regardless of solubilizer type. Luminescence lifetimes of 530 QDs were found to be 10.5 ns for both chirality types (Table 4.2).

Table 4.2. Spectral luminescent parameters of chiral nanostructures in aqueous solutions

NC	Quantum yield, %	$\langle\tau\rangle$, ns
580 QDs, L-cys	1.3	2.16
580 QDs, D-cys	1.2	2.25
620 DiRs, L-cys	1.6	1.6
620 DiRs, D-cys	1.6	1.6
530 QDs, L-cys	5	10.5
530 QDs, D-cys	5	10.5

It is very likely that luminescence of all three types of nanostructures is quenched during thiol solubilization as a result of hole transfer from the NS to the thiol group [54]; it is supported by the fact that luminescence lifetimes of the nanostructures decrease. The extent of luminescence quenching in the nanostructures did not depend of chirality type of the solubilizer.

4.5. Investigation of luminescent properties of chiral NCs in biological media

For investigating stability of nanostructures in biological media we chose nutrition media DMEM and DMEM with protein serum, because this medium is a suitable model of a biological object. The study of NC interaction with these media was conducted using 620 DiRs. We registered NC luminescence spectra in nutrition media, shown on Figure 4.19.

A **B**

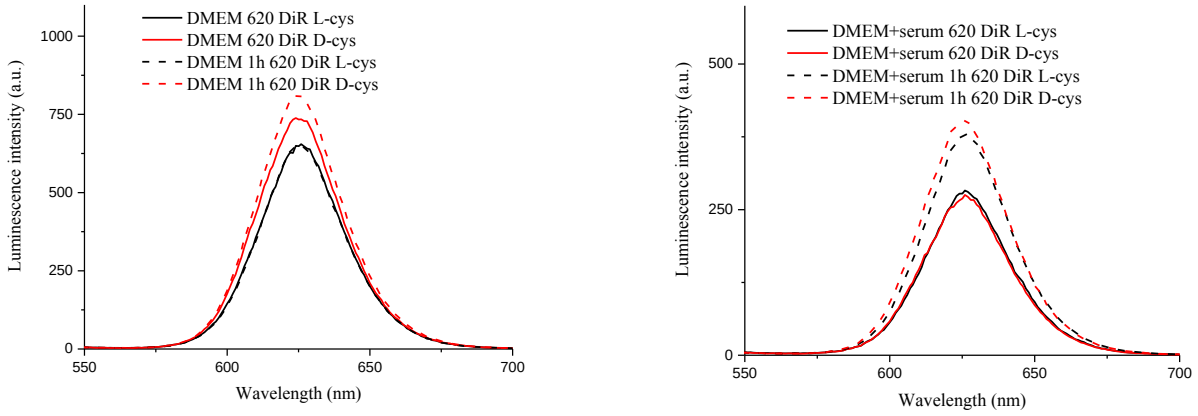

Figure 4.19 Luminescence spectra of chiral 620 DiRs in DMEM medium (A) and DMEM medium with serum (B) excited by 450 nm light

Our spectral-luminescent analysis has uncovered that in the DMEM nutrition medium a luminescence rise appears in 620 DiRs compared to the nanostructures in water. The rise was independent of solubilizer type; however it was higher for D-cysteine capped 620 DiRs. During the repeated measurements after 1 hour, the

luminescence rise of approximately 10% was observed for D-cysteine capped nanostructures, with no change of intensity for nanostructures with L-cysteine. Repeating the experiment in DMEM medium with serum led to luminescence quenching in the nanostructures, halving its intensity compared to luminescence in DMEM. Luminescence of 620 DiRs in DMEM medium with serum rose again after an hour, demonstrating approximately 35% intensity increase in L-cysteine capped nanostructures and 50% in D-cysteine capped nanostructures. It can possibly be explained by enantioselective interaction in the system between the medium components, the chiral nanostructures, and the leftovers of free solubilizer molecules.

In order to analyze luminescence decay kinetics in the samples and to study spatial distribution of the luminescent particles in the sample FLIM (Fluorescence-lifetime imaging microscopy) images were recorded in DMEM and DMEM with serum media within a 60 minute interval, as presented on Figure 4.20.

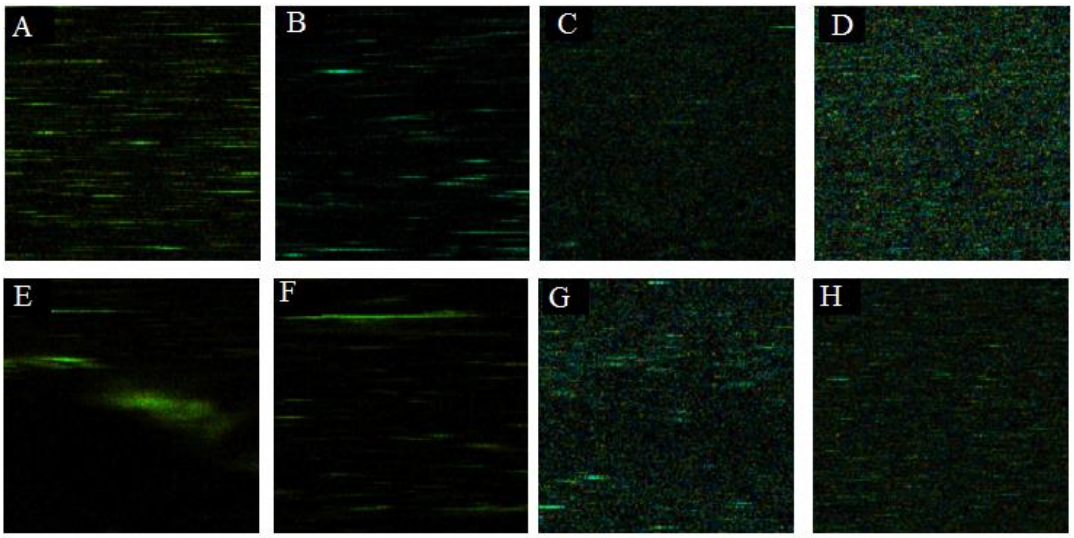

Figure 4.20. FLIM images of chiral DiRs in DMEM medium and DMEM medium with serum: A-B: 620 L-cysteine capped DiRs in DMEM medium with 60 minute interval; C-D: 620 L-cysteine capped DiRs in DMEM medium with serum with 60 minute interval; E-F: 620 D-cysteine capped DiRs in DMEM medium with 60 minute interval; G-H: 620 D-cysteine capped DiRs in DMEM medium with serum with 60 minute interval.

According to FLIM date, nanostructure aggregates can be seen in all sample types in the form of luminescent ensembles. Conceivably, adding the serum to the nutrition media leads to a decrease in nanoparticle aggregation ability, since we observed less luminescent ensembles. A multi-exponential luminescence decay model was used for determining 620 DiRs luminescence lifetime in the nutrition medium. Two-exponential dependence (Equation 3.7) was used for approximation, and mean luminescence decay times were calculated with Equation 3.8. The approximation results are shown in Table 4.3.

Table 4.3. Luminescence decay times of chiral nanostructures in biological media

NC	Amplitude A_1, %	τ_1, ns	Amplitude A_2, %	τ_2, ns	$\langle\tau\rangle$, ns
DMEM DiR L-cysteine	50±10	3.8	50±10	3.2	3.5
DMEM DiR L-cysteine 1 hour	50±10	3.8	50±10	3.2	3.5
DMEM DiR D-cysteine	50±10	3.11	40±10	5.05	4.3
DMEM DiR D-cysteine 1 hour	50±10	4.4	50±10	5.32	4.9
DMEM+serum DiR L-cysteine	50±10	2.5	50±10	2.13	2.4
DMEM+serum DiR L-cysteine 1 hour	30±20	4.8	70±20	2.14	3.5
DMEM+serum DiR D-cysteine	40±10	2.31	50±10	2.12	2.2
DMEM+serum DiR D-cysteine 1 hour	50±10	4.44	50±10	2.76	3.9

During the processes of nanostructure incorporation into biological media, the luminescence decay times of 620 DiRs increased. However, using DMEM nutrition medium with serum resulted in a decrease in luminescence lifetimes in nanostructures regardless of solubilizer type. Along with this, a temporal increase of luminescence lifetimes of 620 DiRs is observed regardless of the solubilizer and medium type.

It can be assumed that introduction of the serum into the nutrition medium yet leads to formation of nanostructure aggregates, which are afterwards dissolved due to a certain form of interaction with the serum. This assumption is indirectly supported by a more significant (percentagewise) temporal luminescence rise in nanostructures situated in nutrition media with the serum: 35% for L-cysteine capped and 50% for D-cysteine capped 620 DiRs compared to 0% and 10%, respectively, in nutrition media without the serum.

4.6 Conclusions

The studies of chiral semiconductor nanocrystal optical properties have demonstrated the following:

- Chiral nanostructures based on 580 QDs, 620 DiRs and 530 QDs were formed during solubilization processes of nanocrystals with L- and D-cysteine.
- Luminescence decay times and quantum yields of all types of nanostructures decrease during nanostructures solubilization with chiral L- and D-cysteine enantiomers, probability due to hole transfer from the nanostructures to the thiol group of cysteine molecules on the NC surface.
- During the processes of nanostructure introduction into biological media, the luminescence decay times of 620 DiRs increased, however, using DMEM nutrition medium with serum resulted in a decrease in

luminescence decay times in 620 DiRs for all solubilizer types. A significant temporal increase of luminescence decay times in nutrition media with serum indicates the destruction of chiral nanostructure aggregates.

5 Enantioselective uptake of CdSe/ZnS QDs by EAC cells

Below we present the results of *in vitro* study of chiral nanostructures optical properties in the living cells of Ehrlich ascites carcinoma (EAC) in mice using 530 CdSe/ZnS QDs as an example.

5.1. Investigation of chiral CdSe/ZnS QDs spectral luminescent properties in EAC cells

As shown in the previous chapter, water-soluble chiral nanocrystals can be fabricated as a result of CdSe/ZnS nanocrystals phase transfer from the organic phase to the aqueous in the presence of cysteine enantiomers. 530 CdSe/ZnS QD cellular uptake by the living Ehrlich ascites carcinoma cells was performed using the method described in Chapter II. Luminescent images of EAC cells incubated with L- or D-cysteine 530 CdSe/ZnS QDs during 3, 6, 24 or 48 hours are shown on Figure 5.1.

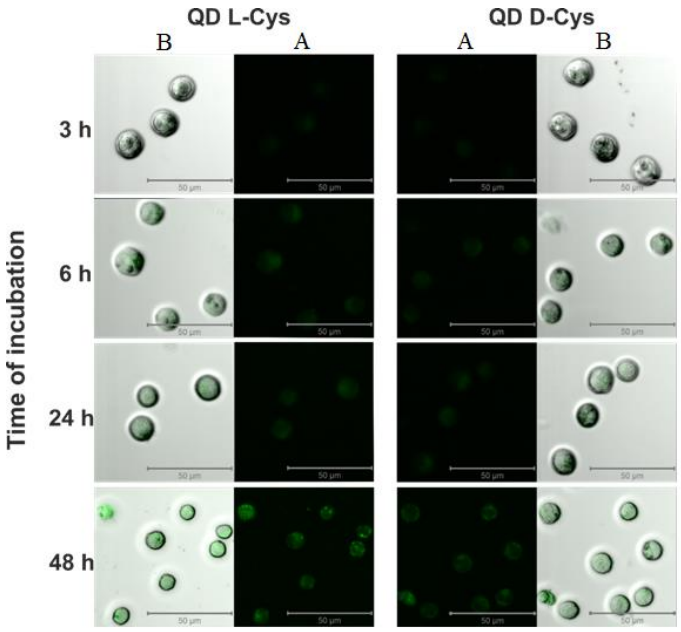

Figure 5.1. Luminescent images of incubated with L,D-cysteine 530 QD nanostructure ensembles (A) and pictures acquired by overlapping the luminescent signals on cell images (B). The signals were measured after 3, 6, 24 and 48 hours of incubation, respectively.

530 QDs luminescence was excited by 405 nm light and registered in 500-560 spectral band, corresponding to 530 QD luminescence band.

The luminescent images in Figure 5.1 confirm cellular uptake of 530 QDs. The areas with significantly higher luminescence intensity than in the other cell parts indicate the formation of cellular bubbles – vesicles. We observed a gradual increase of 530 QDs luminescence intensity in the cells for both chiral forms during incubation. Luminescent images analysis (Figure 5.1) has shown that quantum dot luminescence intensity with L-cysteine was higher than with D-cysteine during all incubation periods.

The luminescent images of chiral 530 QDs (Figure 5.2) demonstrate that the luminescence intensity of L-cysteine capped 530 QDs in EAC cells is significantly higher than that of D-cysteine capped QDs by the end of 96 hour incubation.

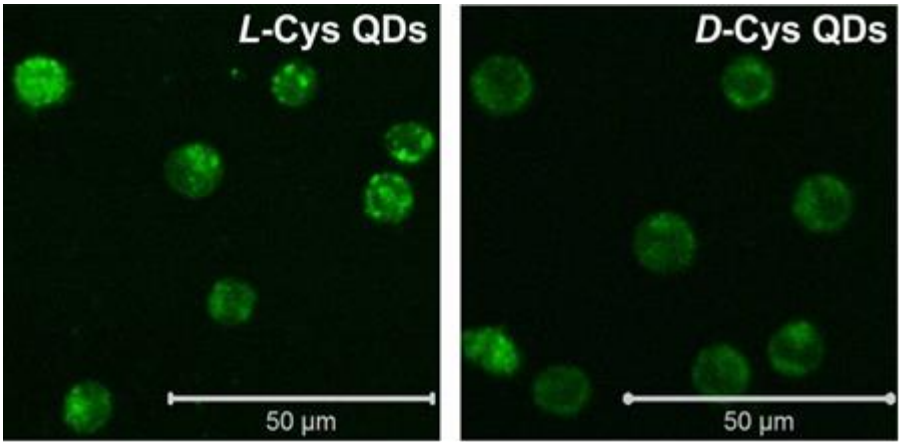

Figure 5.2. Luminescent images of EAC cells with D- and L-enantiomer capped 530 QDs after 96 h of incubation

We recorded luminescence spectra of chiral 530 QDs in cells. Luminescence spectra and mean luminescence intensities of 530 QDs in EAC cells are depicted on Figure 5.3. Mean luminescence intensity values were calculated based on luminescence intensities of nanocrystal ensembles in several cells.

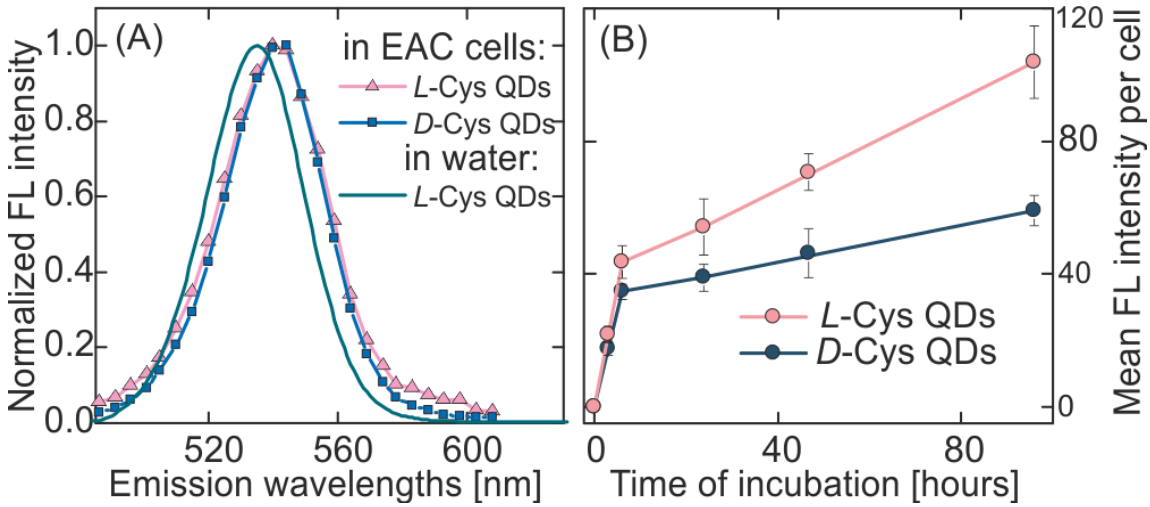

Figure 5.3. Spectral luminescent parameters of L- and D-cysteine capped 530 QDs: A: Luminescence spectra of 530 QDs in water and EAC cells after 96 hours of incubation; B: mean luminescence intensity of 530 QDs in the cells versus incubation time.

It can be seen from Figure 5.3 that firm localization of QDs in cellular vesicles leads to a red shift of the QD luminescence band with respect to its position in aqueous solution. This may be caused by dot-to-dot energy transfer through FRET mechanism [55] in case of low distances between NC in cell vesicles. Luminescence intensity (I) is proportional to a product of quantum yield (φ_{QD}), extinction coefficient (ε) and concentration of nanostructures (C): $I \sim \varphi_{QD} \cdot \varepsilon \cdot C$. Since the luminescence intensity of L-cysteine capped QDs in a single cell is two times higher than that of D-cysteine capped QDs after 96 hours of incubation, it can be caused either by concentration of the nanocrystals introduced into cells, or by unequal luminescence quantum yields. In order to answer this question, we should study the luminescence kinetics of 530 QDs in EAC cells.

5.2. Luminescence kinetics of 530 QDs in EAC cells

For studying 530 QD stability and investigating the reason for luminescence intensity increase of 530 QD ensembles in EAC cells, QD luminescence decay times

were measured. Luminescence decay curves for chiral 530 QDs in EAC cells are shown on Figure 5.4. Decay curves of the initial hydrophobic QDs and the QDs in water solution are given for reference.

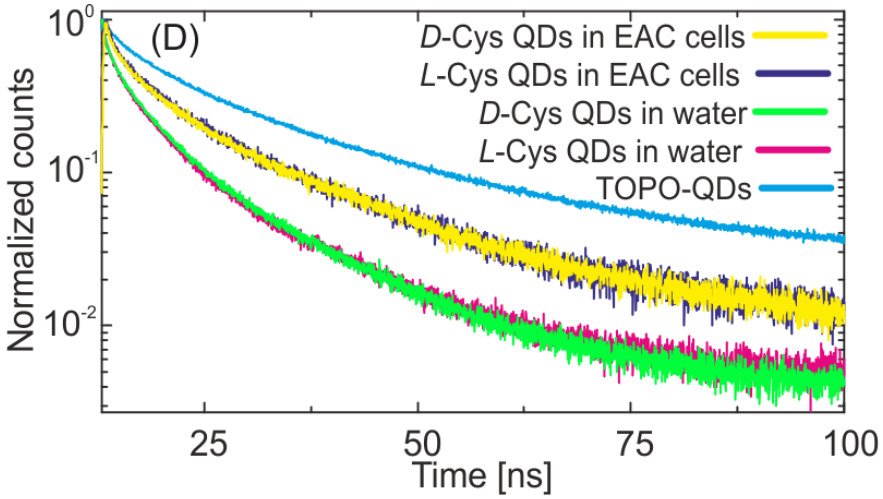

Figure 5.4. Luminescence decay curves of L- and D-cysteine capped 530 QDs in EAC cells, in water and initial 530 QDs in toluene. A bandpass filter centered at 530 nm was used for luminescence registration.

We used a three-exponential function (Equation 3.7) for approximating the luminescence decay curves of nanostructures. 530 QDs mean luminescence decay time was calculated using Equation 3.8. Luminescence lifetime of L- and D-cysteine capped 530 QDs in cells appeared to be equal for almost all incubation periods; mean luminescence decay times were found to be 15 ns and 16 ns, respectively.

Luminescence quantum yield (φ) of nanocrystals is proportional to luminescence lifetime (τ) and energy transition radiative constant (k_r)

$$\varphi = \tau \cdot k_r \tag{5.1}$$

Therefore, due to very close luminescence lifetimes and assuming the radiative constant to be unaltered we come to a conclusion that luminescence quantum yields of chiral nanocrystals in cells are almost equal. This fact indicates the absence of enantioselective fluorescence quenching upon 530 QD incorporation into the cells and enables the use of luminescence intensity to estimate the chiral QD relative concentration inside the cells. It means that concentration of the incubated L-cysteine

capped 530 QDs is higher than the concentration of D-cysteine capped QDs, bearing evidence of enantioselective cellular uptake of nanocrystals in EAC cells.

5.3 Conclusions:

- We have studied luminescence intensities and decay times of chiral 530 QDs in the living cells of Ehrlich ascites carcinoma.
- Due to very close QD luminescence lifetimes and assuming the radiative constant of QDs to be unaltered we came to a conclusion that the luminescence intensity of 530 QDs in cells allows to determine relative QD concentrations in EAC cells. L-cysteine capped 530 QD concentration in EAC cells after 96 hours of incubation was found to be two times higher than of D-cysteine capped QDs.

6 The study of interaction between nanostructures and photosensitizer molecules

As shown in the previous chapter, the chirality of CdSe/ZnS QDs may have a significant impact on their living EAC cells penetration efficiency, indicating that QD chirality can largely affect their interaction efficiency with chiral molecules.

Chlorin e6, used today in clinical practice as a PDT photosensitizer, is an L-enantiomer of the chiral molecule. For this reason, it is of interest to investigate the influence of nanostructure chirality type, namely for L- and D-cysteine stabilized CdSe/ZnS DiRs, on their interaction efficiency with chlorin e6 molecules.

In this chapter we describe interaction of chiral nanostructures with photosensitizer chlorin e6 molecules in DMSO solution. In our experiments we used chiral 620 DiRs that were proved to be stable in biological media.

6.1. Spectral luminescent properties of chiral nanostructures mixtures with photosensitizer molecules

We investigated spectral luminescent properties of chiral 620 DiR mixtures with chlorin e6 photosensitizer molecules in DMSO that allowed NC/chlorin e6 complex formation. The test samples were fabricated by increasing chlorin e6 concentration in L- and D-cysteine capped 620 DiR solutions with ratios 1:1, 2:1, 3:1, 15:1, 50:1, 100:1. Absorption spectra of the samples are shown on Figure 6.1.

A

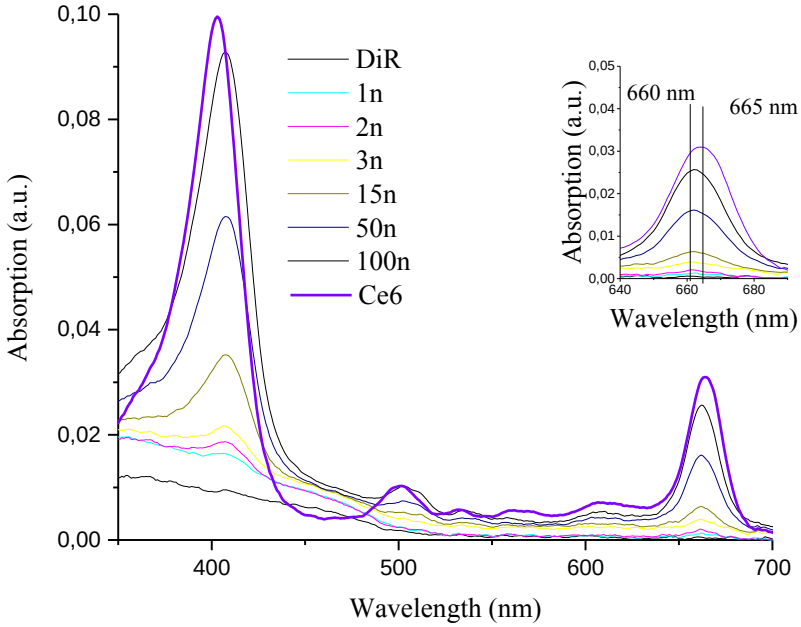

B

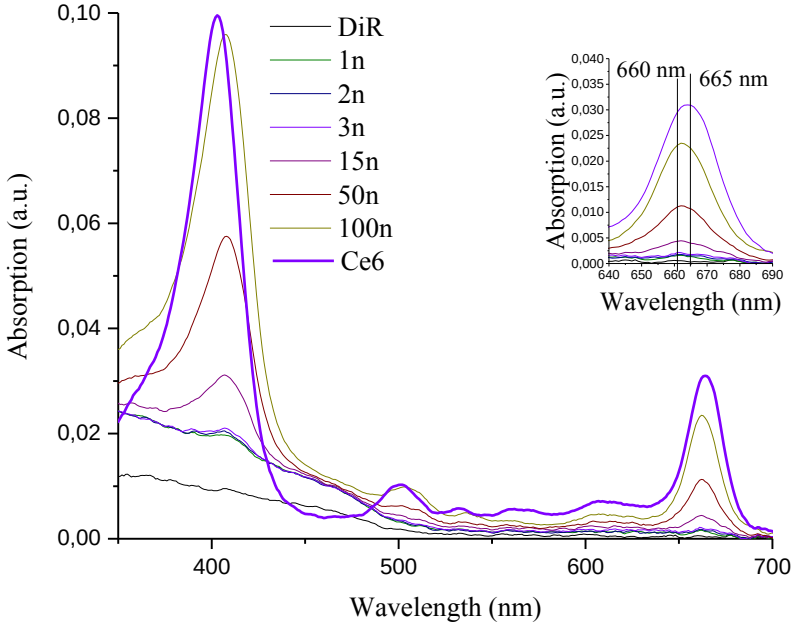

Figure 6.1. Absorption spectra of 620 DiR / chlorin e6 mixtures with L-cysteine (A) and D-cysteine (B) capped nanostructures with different concentrations (*n*) of chlorin e6 and 620 DiRs, respectively 1:1, 2:1, 3:1, 15:1, 50:1, 100:1. Solvent – DMSO.

Alteration of the first chlorin e6 absorption band *Q* (I) (~660 nm) is observed in the absorption spectra. It undergoes a 5 nm hypsochromic shift, indicating a possible form of free chlorin and bound into complex with 620 DiRs. Analysis of chlorin e6 absorption spectra in NC mixtures showed that chlorin e6 spectra in mixtures with different nanostructure enantiomers were identical. It means that the chirality type of NCs does not affect chlorin e6 spectral form.

The collected experimental data of chlorin e6 absorption in mixed solutions with L- and D-cysteine capped 620 DiRs indicates formation of 620 DiR/chlorin e6 complexes in DMSO, presumably due to hydrogen bonding.

The registered luminescence spectra of 620 DiR/chlorin e6 mixtures excited by 450 nm radiation are shown on Figure 6.2.

A B

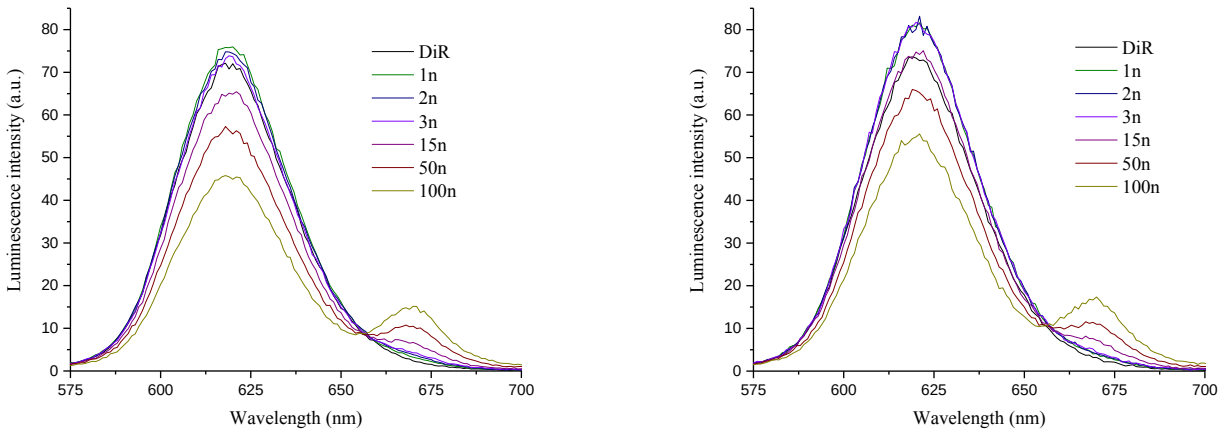

Figure 6.2. Luminescence spectra of 620 DiR/ chlorin e6 mixtures with L-cysteine (A) and D-cysteine (B) capped nanostructures with different concentrations (*n*) of 620 DiRs and chlorin e6, 1:1, 2:1, 3:1, 15:1, 50:1, 100:1 respectively, excited by 450 nm light.

620 DiRs luminescence rise is observed in the samples luminescence spectra from the first addition with concentration ratio 1:1. It demonstrates 620 DiRs luminescence susceptibility to changes in the environment. Further increase of chlorin e6 concentration in 620 DiRs mixed solution led to a decrease in DiR luminescence

intensity and an appearance of another band centered at ~ 670 nm. It can also be seen that increasing concentration of chlorin e6 in the mixed solution does not induce any change in 620 DiR luminescence band. A gradual luminescence quenching of 620 DiRs was observed after the first addition for both solubilizer chirality types, however in case of L-cysteine the luminescence quenching efficiency in nanostructures was somewhat higher.

For studying spectral luminescent properties of chlorin e6/NC mixture we registered luminescence spectra excited by 640 nm light, when only chlorin e6 is excited. Absorption of 620 DiRs in this area is negligible, therefore all registered luminescence intensity corresponds exclusively to intrinsic absorption of chlorin e6 in this spectral region. Luminescence spectra of the samples are shown on Figure 6.3.

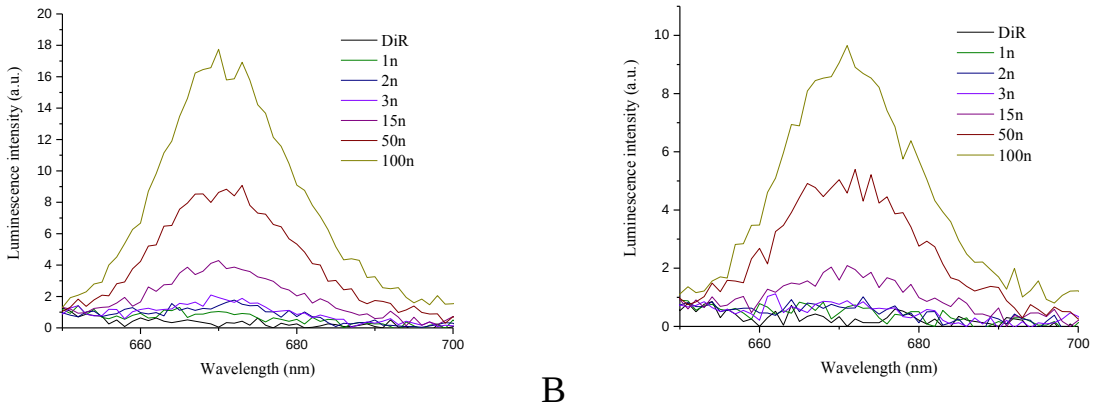

Figure 6.3. Luminescence spectra of 620 DiR / chlorin e6 mixtures with L-cysteine (A) and D-cysteine (B) capped nanostructures with different concentrations (n) of 620 DiRs and chlorin e6, 1:1, 2:1, 3:1, 15:1, 50:1, 100:1 respectively, excited by 640 nm light.

Starting with the first addition, a gradual proportional increase in photosensitizer luminescence intensity is observed for both 620 DiRs chirality types. Spectral parameter analysis revealed a gradual decrease in luminescence quantum yield of 620 DiRs and chlorin e6.

Figure 6.4 illustrates exponential dependence of 620 DiR relative luminescence intensity quenching on the components concentration ratio in the mixture ($n = C_{clorin\ e6}/C_{620\ DiR}$).

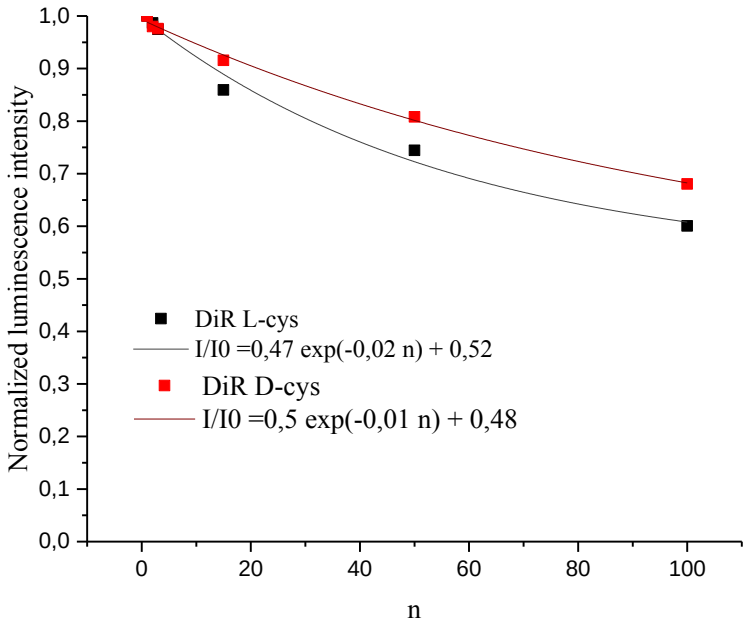

Figure 6.4. Dependence of 620 DiRs relative luminescence intensity on concentration ratio ($n = C_{clorin\ e6}/C_{620\ DiR}$) in a 620 DiR mixed solution with chlorin e6.

In our case the experimental data is approximated by an exponential function $y = 0{,}47 \cdot \exp(-0.02 \cdot n) + 0{,}52$ for the L-cysteine system, and $y = 0{,}5 \cdot \exp(-0.01 \cdot n) + 0{,}48$ for the D-cysteine system. The fact that the exponential factor is ~ 0.01 indicates that a single Ce6 molecule weakly quenches the luminescence of a single 620 DiR. Under the conditions of this experiment such situation may be observed when a large number of 620 DiRs remain in a state free from photosensitizers. It is also worth mentioning that 620 DiR/chlorin e6 complexes form better, thus favoring enantioselective of the system.

6.2. Study of energy transfer efficiency in 620 DiR/chlorin e6 system

According to Förster theory, two conditions must apply simultaneously for effectively transferring energy by FRET mechanism for a given donor-acceptor pair:

1) The distance between a donor and an acceptor must not exceed the critical radius (R_0).

2) The acceptor absorption spectrum must overlap with the donor luminescence spectrum. Overlap integral of these two spectra, shown on Figure 6.5, affects the energy transfer efficiency.

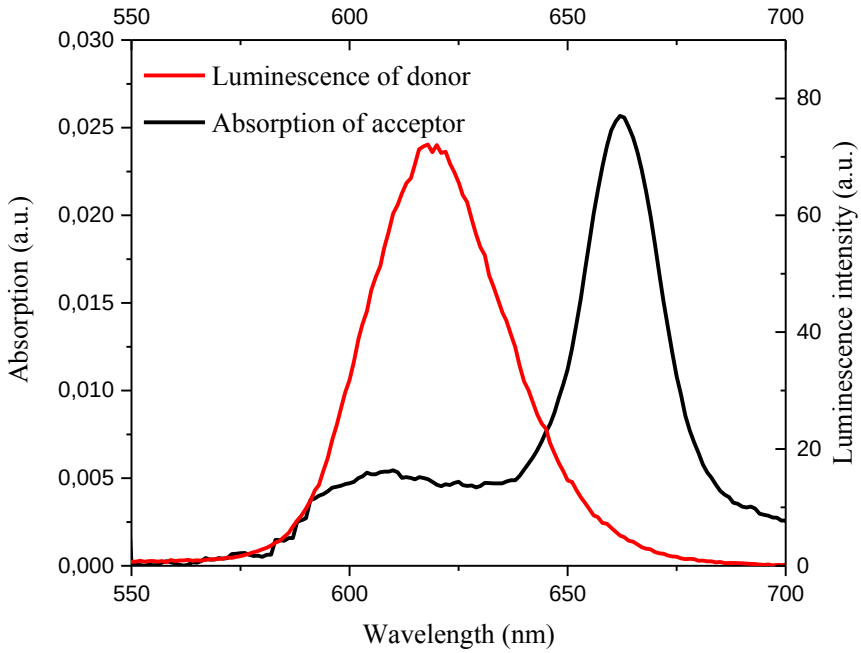

Figure 6.5. Absorption and luminescence spectra of the 620 DiR – chlorin e6 donor-acceptor pair.

Overlap integral of the acceptor absorption spectrum and the donor luminescence spectrum is calculated using the following equation:

$$I = \int I_D^N(\nu) \cdot \varepsilon_A(\nu) \cdot \nu^{-4}\, d\nu \tag{6.1}$$

It is of order ($M^{-1}cm^3$) for systems with both enantiomeric forms.

A distance between a donor and an acceptor at which the energy transfer efficiency by FRET mechanism is 50% can be calculated using:

$$R_0^6 = \frac{9000 \cdot ln10 \cdot \Phi^2 \cdot QY_{0D} \cdot I}{128 \cdot \pi^5 \cdot n^4 \cdot N}, \quad (6.2)$$

where QY_{0D} = 0,21 is the donor luminescence quantum yield without a quenching agent, N = 6,022 $\cdot 10^{23}$ mol^{-1} is Avogadro constant, n = 1,47 is refractive index of DMSO, $\Phi^2 = {}^2/_3$ is the orientation factor, I is the overlap integral. Therefore, the critical radius is R_0 = 4.95 nm.

By Förster's equation, the transfer efficiency is calculated as:

$$E_t = \frac{1}{1 + \left(\frac{R_{DA}}{R_0}\right)^6}, \quad (6.3)$$

where R_{DA} is the distance between a donor and an acceptor.

The form of DiR nanostructures allows to assume two possible core positions with respect to the rod-shaped shell, leading to different distances between donors and acceptors.

Let us consider two models of CdSe core positioning in the rod-shaped CdS shell. Schematic images of these 620 DiRs are shown on Figure 6.6.

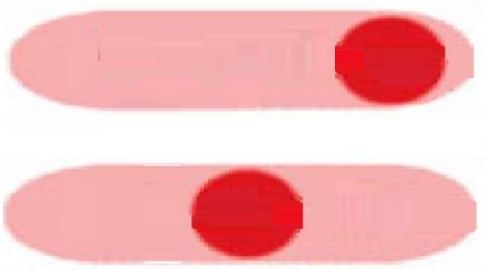

Figure 6.6. Schematic representation of 620 DiRs

Chlorin e6 can attach to any point of the 620 DiR shell surface.

Because the sizes of nanostructures are 4 nm in diameter and 10 nm in length, according to electron microscopy data, mean distances from the photoexcitation energy

donor (core) to the acceptor (photosensitizer molecule) are approximately 3.2 nm in case of central positioning of the CdSe core, and 5.5 nm in case of its localization at one of the end points.

Therefore, theoretical values of energy transfer efficiency calculated from the Equation 6.3 reach 34% when the core is situated at one of the shell end points, and 93% when the CdSe core is situated in the center.

It does not seem possible to determine energy transfer efficiency per one donor-acceptor pair experimentally due to an uncertainty of CdSe cores position in the CdS shells and of Ce6 fraction bound into complex with NC in the mixtures.

However it should be noted that the energy transfer efficiency in the studied samples can be analyzed using luminescence excitation spectra of Ce6 in mixtures with NC enantiomers. Luminescence excitation spectra of 620 DiRs and chlorin e6 in different concentrations with registration wavelength 680 nm are shown on Figure 6.7. We performed normalization by the amplitude of the first chlorin e6 absorption band, that corresponds to normalization by luminescence quantum yield of chlorin e6 and by its concentration. It allowed us to directly analyze the energy transfer efficiency from the nanostructures to photosensitizer molecules judging by contribution of the nanocrystals absorption spectrum into the chlorin e6 luminescence excitation spectrum.

A

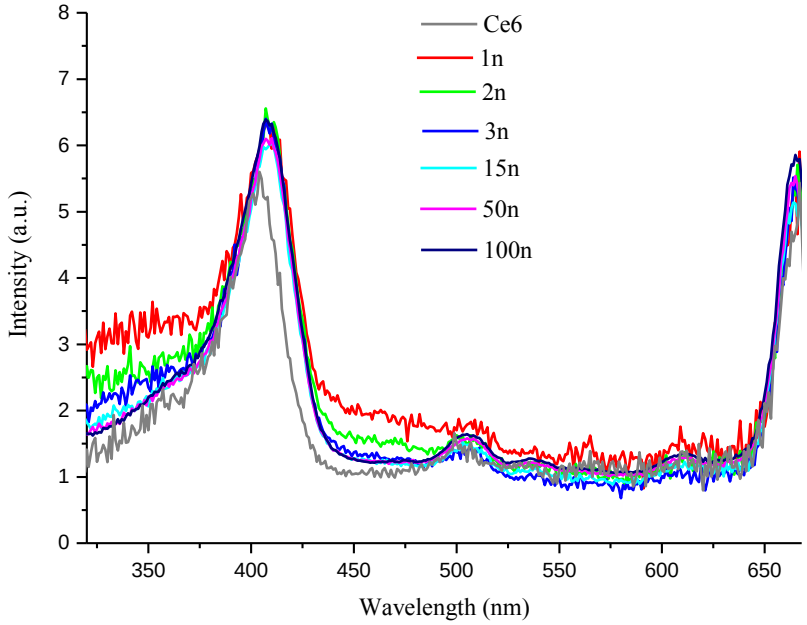

B

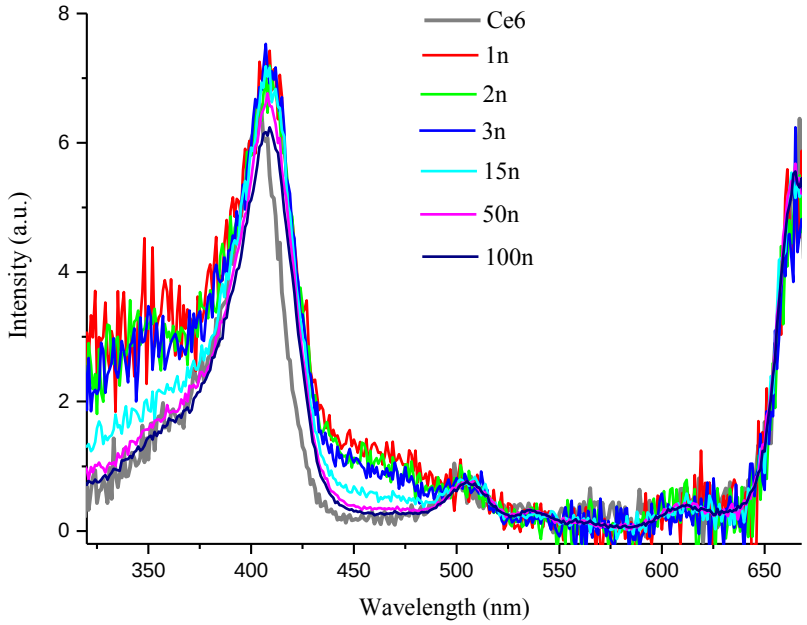

Figure 6.7. Luminescence excitation spectra of 620 DiR – chlorin e6 complexes (registration wavelength 680 nm) with chlorin e6 to 620 DiRs ratios (n) 1:1, 2:1, 3:1, 15:1, 50:1, 100:1; free chlorin e6 excitation spectrum.

Comparing chlorin e6 luminescence excitation spectrum with the luminescence excitation spectra of chlorin e6 mixed with 620 DiRs, it can be seen that the luminescence excitation spectra of the chlorin e6 mixture with 620 DiRs considerably differ in form from the absorption spectrum of free chlorin e6. The cause of this difference is the contribution of nanostructure absorption spectrum at 300-500 nm band to the excitation spectra of chlorin e6 mixed with 620 DiRs. It confirms the existence of energy transfer from chiral nanostructures to photosensitizer molecules.

We calculated Ce6 sensitized luminescence normalized intensity using the luminescence excitation spectra of Ce6 mixtures with chiral NCs:

$$I_{\text{sensitizer}} = \frac{I_{\text{registered}} - I_{\text{intrinsic}}}{I_{\text{intrinsic}}}, \tag{6.4}$$

where $I_{\text{sensitizer}}$ is normalized sensitized luminescence intensity of chlorin e6, $I_{\text{registered}}$ is the registered chlorin e6 luminescence, $I_{\text{intrinsic}}$ is the intrinsic luminescence of chlorin e6.

The dependence of normalized Ce6 sensitized luminescence on its relative concentration in the mixtures with enantiomers of chiral NCs is shown on Figure 6.8.

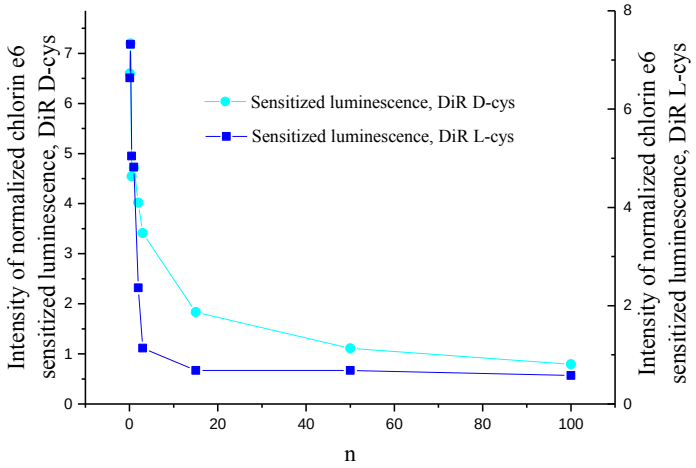

Figure 6.8. Intensity of normalized chlorin e6 sensitized luminescence associated in a complex with chiral 620 DiRs at different concentration ratios.

The sensitized luminescence ($I_{sensitizer}$) is proportional to a product of chlorin e6 luminescence quantum yield (φ_{Ce6}), FRET efficiency (E_t) and concentration of photoexcitation energy donors (C_{DiR}), associated in a complex:

$$I_{sensitizer} \sim \varphi_{Ce6} \cdot E_t \cdot \mathrm{C}_{DiR}, \tag{6.5}$$

Intrinsic luminescence intensity ($I_{intrinsic}$) of chlorin e6 is proportional to a product of chlorin e6 luminescence quantum yield (φ_{Ce6}) and concentration of photoexcitation energy donors associated in a complex (C_{DiR}):

$$I_{intrinsic} \sim \varphi_{Ce6} \cdot \mathrm{C}_{DiR} \tag{6.7}$$

The dependences shown on Figure 5.6 demonstrate that in both chiral systems an increase in relative concentration (n) results in a decrease of sensitized luminescence intensity. In the mixture with D-cysteine capped DiRs with chlorin e6/DiRs concentration ratios 3:1 (n=3) chlorin e6 sensitized luminescence intensity is two times higher compared to chlorin in a mixed solution with L-cysteine capped DiRs. In the mixture with L-cysteine capped DiRs a more rapid decay dynamics of sensitized luminescence compared to the mixture with D-cysteine capped DiRs, indicating enantioselective interaction of chiral nanostructures with chlorin e6.

The observed inequality in chlorin e6 sensitized luminescence intensity in NC mixtures of different chirality types with the same n can be attributed to the following:

1. Different photoexcitation energy transfer efficiencies (FRET) for complexes with 1:1 stoichiometry, equal luminescence quantum yields of donors (NCs) and similar D-A distances in the complexes.

2. Luminescence quantum yields of the nanostructure enantiomers differ, therefore leading to distinct transfer efficiencies according to Förster's theory.

3. There is a different percentage of NC/Ce6 complexes in the samples at the fixed value of n.

It is worth noting that until today no studies of NC chirality type influence on the energy transfer constant in NC/molecule complexes has been performed. However, it seems unlikely. It was shown in Chapter III that luminescence quantum yields of L- and D- DiRs are almost equal. Thus, the most likely reason for the observed difference in Ce6 sensitized luminescence intensity in the mixtures with chiral NCs is, in our opinion, the distinct concentration of NC/Ce6 complexes with the same *n*; i.e. this difference shows enantioselective interaction of chiral NCs with chiral Ce6 molecules, as a result of which Ce6 is bound with the D-enantiomer of DiR more efficiently.

6.3 Conclusions

- In both systems an increase of *n* is accompanied by a decrease of sensitized luminescence of chlorin e6, which can be related to a decrease in percentage of chlorin e6 associated in a complex with chiral 620 DiRs, because this value is normalized on luminescence quantum yield and Ce6 concentration for any particular *n*;
- Different decay rate of sensitized luminescence directly indicates unequal binding efficiency of chlorin e6 with 620 DiRs of different chirality types. Enantioselective binding of D-cysteine capped 620 DiRs with levorotatory chlorin e6 photosensitizer molecules is a very likely possibility.
- It does not seem possible to determine the percentage of chlorin e6 bound into complex with NC, and therefore the transfer efficiency calculated per single donor-acceptor pair. Further investigation is required on this matter. In particular, in course of such experiments it is necessary to control the size of nanostructures in order to eliminate the influence of aggregation on energy transfer efficiency from 620 DiRs to chlorin e6.

7 Summary

In this work chiral nanostructures based on CdSe/ZnS quantum dots (QD) and CdSe/CdS quantum dots in quantum rods (DiR), solubilized by L- and D-cysteine were formed using nanocrystal phase transfer method from organic to the aqueous phase. We studied photophysical properties of chiral nanostructures in different biological media and analyzed spectral luminescent properties of complexes based on chiral nanostructures.

The results of this work may be summed up as follows:

1. Chiral nanostructures with CdSe/ZnS QDs and CdSe/CdS DiRs capped with L- and D-cysteine were fabricated, which was confirmed by registering IR absorption and circular dichroism spectra.
2. According to electron microscopy data, the nanostructures are aggregated to some extent after solubilization. Aggregation is enhanced as a result of chiral nanostructures transfer to biological nutrition media. However, the nanostructures in nutrition media remain temporally stable. DMEM with serum was determined as the optimal culture medium.
3. The influence of CdSe/ZnS quantum dots chirality on their cellular uptake was studied using the living Ehrlich ascites carcinoma cells. It was found that chirality affects the cellular uptake efficiency of nanostructures. A comparative analysis of fluorescence intensities and lifetimes in L- and D-cysteine capped QDs in cells has revealed enantioselective cellular uptake of nanostructures, namely that L-cysteine capped QDs uptake is higher than that of D-cysteine capped QDs. We believe this principle may lay the groundwork for novel approaches to studying biological objects and to application of nanostructures in medicine.
4. It was found that enantioselective binding of D-cysteine capped 620 DiRs with levorotatory chlorin e6 photosensitizer molecules takes place during the formation process of chiral 620 DiR complexes with chlorin e6.

The results of this work, presented in Chapter IV, are published in the following paper:

Martynenko I.V., Kuznetsova V.A., Litvinov I.K., Orlova A.O., Maslov V.G., Fedorov A.V., Dubavik A., Purcell-Milton F., Gun'ko Y.K., Baranov A.V. "Enantioselective cellular uptake of chiral semiconductor nanocrystals" // Nanotechnology - 2016, Vol. 27, No. 7, pp. 075102-(1-8)

The results of this work, presented in Chapter V of the dissertation, are published in the following paper:

Литвинов И.К., Кузнецова В.А., Орлова А.О., Исследование фотофизических свойств комплексов полупроводниковых квантовых стержней селенида кадмия и хлорина е6 // Сборник материалов IV-го Всероссийского конгресса молодых ученых, СПб, Университет ИТМО, 2015.

"Litvinov I.K, Kuznetsova V.A., Orlova A.O., Investigation of photophysical properties of complexes formed by semiconductor cadmium selenide quantum rods and chlorin e6 // IV All-Russian congress of young scientists technical digest, Saint Petersburg, ITMO University, 2015 (in Russian)."

8 References

[1] Shirin Ghaderi, Bala Ramesh, and Alexander M. Seifalian, Fluorescence nanoparticles “quantum dots” as drug delivery system and their toxicity: a review, Journal of Drug Targeting 19(7) (2011) 475.

[2] Abhilash, M., Potential applications of Nanoparticles, International Journal of Pharma and Bio Sciences V1(1) (2010).

[3] Huda Yusuf , Whan-Gi Kim , Dong Hoon Lee, A Hierarchical Self-Assembly Route to Three-Dimensional Polymer−Quantum Dot Photonic Arrays, Langmuir 23 (10) (2007) 5251.

[4] Alireza Valizadeh, Haleh Mikaeili, Mohammad Samiei, Quantum dots: synthesis, bioapplications, and toxicity, Nanoscale Research Letters 7:480 (2012).

[5] Noda Y, Noro S, Akutagawa T, Nakamura T, Gold nanoparticle assemblies stabilized by bis(phthalocyaninato)lanthanide(III) complexes through van der Waals interactions, Sci Rep. 4 (2014) 3758.

[6] Xiwen Gong, Zhenyu Yang, Grant Walters, Highly efficient quantum dot near-infrared light-emitting diodes, Nature Photonics 10 (2016) 253.

[7] R.J. Byers, E. R. Hitchman, Quantum Dots Brighten Biological Imaging, Progress in Histochemistry and Cytochemistry 45 (2011) 201.

[8] Peng XG, Manna L, Yang WD, Wickham J, Scher E, Kadavanich A, Alivisatos A, Shape control of CdSe nanocrystals, Nature 404 (2000) 59.

[9] Dmitri V. Talapin, James H. Nelson, Elena V. Shevchenko, Shaul Aloni, Bryce Sadtler, and A. Paul Alivisatos, Seeded Growth of Highly Luminescent CdSe/CdS Nanoheterostructures with Rod and Tetrapod Morphologies, Nano letters 7 (2007) 2951.

[10] Mokari, T. and U. Banin, Synthesis and Properties of CdSe/ZnS Core/Shell Nanorods, Chemistry of Materials 15(20) (2003) 3955.

[11] Wen, Xiaoming; Sitt, Amit; Yu, Pyng; Ko, Hsien-chen; Toh, Yon-Rui; Tang, Jau, Studies of the photostability of CdSe/CdS dot-in-rod nanoparticles, Journal of Nanoparticle Research 14 (2012) 1278.

[12] А.В. Баранов, В.Г.Маслов, А.О. Орлова, А.В. Федоров Практическое использование наноструктур. Учебное пособие, СПб: НИУ ИТМО 2014.

[13] Громова Ю. А., Мартыненко И.В., Орлова А. О. Практическое использование наноструктур, СПб: НИУ ИТМО 2014.

[14] B. O. Dabbousi, J. Rodriguez-Viejo, F. V. Mikulec, J. R. Heine, H. Mattoussi, R. Ober, K. F. Jensen, and M. G. Bawendi, ChemInform Abstract: (CdSe)ZnS Core-Shell Quantum Dots: Synthesis and Characterization of a Size Series of Highly Luminescent Nanocrystallites, J. Phys. Chem. 101 (1997) 9463.

[15] Carbone L, Nobile C, De Giorgi M, Sala FD, Morello G, Pompa P, Hytch M, Snoeck E, Fiore A, Franchini IR, Nadasan M, Silvestre AF, Chiodo L, Kudera S, Cingolani R, Krahne R, Manna L, Synthesis and micrometer-scale assembly of colloidal CdSe/CdS nanorods prepared by a seeded growth approach, Nano Lett 7 (2007) 2942.

[16] Brad A. Kairdolf, Andrew M. Smith, Todd H. Stokes, Semiconductor Quantum Dots for Bioimaging and Biodiagnostic Applications, Annual Review of Analytical Chemistry 6 (2013) 143.

[17] Bruchez M Jr, Moronne M, Gin P, Weiss S, Alivisatos AP, Semiconductor nanocrystals as fluorescent biological labels, Science 281 (1998) 2013.

[18] Nadia Anikeeva, Tatiana Lebedeva, and Yuri Sykulev, Quantum dot/peptide-MHC biosensors reveal strong CD8-dependent cooperation between self and viral antigens that augment the T cell response, PNAS 103 (2006) 16846.

[19] Zdobnova TA, Dorofeev SG, Tananaev PN, Vasiliev RB, Fluorescent immunolabeling of cancer cells by quantum dots and antibody scFv fragment, J Biomed Opt. 14(2) (2009).

[20] Lifeng Qi, Xiaohu Gao, Emerging application of quantum dots for drug delivery and therapy, Expert Opin. Drug Deliv. 5(3) (2008) 263.

[21] Xiaohu Gao, Yuanyuan Cui, Richard M Levenson, Leland W K Chung, In vivo cancer targeting and imaging with semiconductor quantum dots, Nature Biotechnology 22 (2004) 969.

[22] Juan Zhou, Yong Yang, and Chun-yang Zhang, Toward Biocompatible Semiconductor Quantum Dots: From Biosynthesis and Bioconjugation to Biomedical Application, Chem. Rev. 115 (21) (2015) 11669.

[23] Xuan Yang, Miaoxin Yang, Bo Pang, Madeline Vara, and Younan Xia, Gold Nanomaterials at Work in Biomedicine, Chem. Rev. 115 (19) (2015) 10410.

[24] Rashmi K Ambasta, Archita Sharma and Pravir Kumar, Nanoparticle mediated targeting of VEGFR and cancer stem cells for cancer therapy, Vascular Cell 3:26 (2011).

[25] Aziliz Hervault and Nguyen Thị Kim Thanh, Magnetic nanoparticle-based therapeutic agents for thermo-chemotherapy treatment of cancer, Nanoscale 6 (2014) 11553.

[26] John H. Phan, Richard A. Moffitt, Todd H. Stokes, Jian Liu, Andrew N. Young,Shuming Nie and May D. Wang, Convergence of biomarkers, bioinformatics and nanotechnology for individualized cancer treatment, Trends Biotechnol. 27(6) (2009) 350.

[27] Rizvi SB, Rouhi S, Taniguchi S, Yang SY, Green M, Near-infrared quantum dots for HER 2 localization and imaging of cancer cells, International Journal of Nanomedicine 9 (2014) 1323.

[28] Urice Tohgha, Krisztina Varga and Milan Balaz, Achiral CdSe quantum dots exhibit optical activity in the visible region upon post-synthetic ligand exchange with D- or L-cysteine, Chem. Commun. 49 (2013) 1844.

[29] Mukhina M.V., Maslov V.G., Baranov A.V., Fedorov A.V., Orlova A.O., Purcell-Milton F., Govan J., Gun'ko Y.K., Intrinsic chirality of CdSe/ZnS quantum dots and quantum rods, Nano Letters 15 (2015) 2844.

[30] F. P. Milton, J. Govan, M. V. Mukhina and Y. K. Gun'ko, The chiral nano-world: chiroptically active quantum nanostructures, Nanoscale Horiz. (2016).

[31] Cintas P, Chirality of living systems: a helping hand from crystals and oligopeptides, Angew. Chem. Int. Ed. Engl (2002).

[32] Taihua Li / Hyun Gyu Park / Hee-Seung Lee et al. Circular dichroism study of chiral biomolecules conjugated with silver nanoparticles, Nanotechnology 15 (2004) 660.

[33] Uwe J. Meierhenrich, Jean-Jacques Filippi, Cornelia Meinert, Jan Hendrik Bredehoft, Jun-ichi Takahashi, Laurent Nahon, Nykola C. Jones, and Søren V. HoffmannCircular Dichroism of Amino Acids in the Vacuum-Ultraviolet Region, Angew. Chem. Int. Ed. 49 (2010) 7799.

[34] Flack, H. D., Louis Pasteur's discovery of molecular chirality and spontaneous resolution in 1848, together with a complete review of his crystallographic and chemical work // Acta Cryst. A65 (2009) 371.

[35] Fu Zhu, Xinyu Li, Yuchen Li, Mei Yan, and Shaoqin Liu, Enantioselective Circular Dichroism Sensing of Cysteine and Glutathione with Gold Nanorods, Anal. Chem., 87 (1) (2015) 357.

[36] Wang, SS; J Chen; L Keltner; J Christophersen; F Zheng; M Krouse; A Singhal, New technology for deep light distribution in tissue for phototherapy, Cancer Journal 8 (2) (2002) 154.

[37] Pawel Mroz, Anastasia Yaroslavsky, Gitika B Kharkwal and Michael R. Hamblin, Cell Death Pathways in Photodynamic Therapy of Cancer, Cancers 3 (2011) 2516.

[38] Glatstein E, Rosenthal DI, Photodynamic therapy: shining light where it is needed // J Clin Oncol. 11(10) (1993) 1844.

[39] Wawrzyńska M, Kałas W, Biały D, Zioło E, Arkowski J, Mazurek W, Strzadała L, In vitro photodynamic therapy with chlorin e6 leads to apoptosis of human vascular smooth muscle cells, Arch. Immunol. Ther. Exp. (Warsz) 58(1) (2010) 67.

[40] What is PDT (Photodynamic Therapy)? (2016, April 4). Retrieved from: Modern Cancer Hospital Guangzhou (MCHG). URL: http://www.moderncancerhospital.com/cancer-treatments/photodynamic-therapy/

[41] R. Rotomskis, J. Valanciunaite b, A. Skripka, S. Steponkiene, G. Spogis, S. Bagdonas, and G. Streckyte, Complexes of functionalized quantum dots and chlorin e6 in photodynamic therapy, Lithuanian Journal of Physics 53 (2013) 57.

[42] Tilahun Ayane Debele, Sydney Peng and Hsieh-Chih Tsai, Drug Carrier for Photodynamic Cancer Therapy, Int. J. Mol. Sci. 16 (2015) 22094.

[43] A. C. S. Samia, X. B. Chen and C. Burda, Semiconductor quantum dots for photodynamic therapy, Journal of the American Chemical Society 125 (2003) 15736.

[44] Jurga Valanciunaite, Andrey S. Klymchenko, Artiom Skripka, Ludovic Richert, Simona Steponkiene, Giedre Streckyte, Yves Melyc and Ricardas Rotomskis, Non-covalent complex of quantum dots and chlorin e6: efficient energy transfer and remarkable stability in living cells revealed by FLIM, RSC Adv. (2014).

[45] Martynenko, V. Kuznetsova, A. Orlova, P. Kanaev, Y. Gromova, V. Maslov, A. Baranov, A. Fedorov, ZnSe/ZnS quantum dots – photosensitizer complexes: optical properties and cancer cell photodynamic destruction effect, Proc. SPIE 9126 Nanophotonics (2014).

[46] Martynenko I.V., Orlova A.O., Maslov V.G., Baranov A.V., Fedorov A.V., Artemyev M. Energy transfer in complexes of water-soluble quantum dots and chlorin e6 molecules in different environments, The Beilstein Journal of Nanotechnology 4 (2013) 895.

[47] Orlova, A.O., et al., Formation of QD-porphyrin molecule complexes in aqueous solutions. Optics and Spectroscopy 105(6) (2008) 889.

[48] A. K. Visheratina, I. V. Martynenko, A. O. Orlova,a) V. G. Maslov, A. V. Fedorov, and A. V. Baranov, Investigation of biocompatible complexes of Mn2+-doped ZnS quantum dots with chlorin e6, J. Opt. Technol. 81 (8) (2014).

[49] Steponkiene S, Valanciunaite J, Skripka A, Rotomskis R, Cellular uptake and photosensitizing properties of quantum dot-chlorin e6 complex: in vitro study, J. Biomed. Nanotechnol. 10(4) (2014) 679.

[50] Evgeny V. Kundelev ; Anna O. Orlova ; Vladimir G. Maslov ; Alexsander V. Baranov ; Anatoly V. Fedorov, Circular dichroism spectroscopy of complexes

of semiconductor quantum dots with chlorin e6, Proc. SPIE 9884, Nanophotonics VI, 988433 (2016).

[51] Pawlukojć A, Leciejewicz J, Ramirez-Cuesta A J and Nowicka-Scheibe, J L-Cysteine: Neutron spectroscopy, Raman, IR and ab initio study, Spectrochimica Acta Part A: Molecular and Biomolecular Spectroscopy 61 (2004) 2474.

[52] Balaž M, Balaž P, Tjuliev G, Zubrík A, Sayagués M, Zorkovská A and Kostova N, Cystine-capped CdSe@ZnS nanocomposites: mechanochemical synthesis, properties, and the role of capping agent, J Mater Sci 48 (2013) 2424.

[53] P. Balaz, R. Jardin, E. Dutková, M.J. Sayagués, M. Baláz, Mechanochemical Synthesis and Characterization of II-VI Nanocrystals: Challenge for Cytotoxicity Issues, Acta Physica Polonica, Series A, (2012).

[54] Sander F. Wuister , Celso de Mello Donega , and Andries Meijerink, Influence of Thiol Capping on the Exciton Luminescence and Decay Kinetics of CdTe and CdSe Quantum Dots, J. Phys. Chem. B 108 (45) (2004) 17393.

[55] Kruchinin S Y, Fedorov A V, Baranov A V, Perova T S and Berwick K, Resonant energy transfer in quantum dots: Frequency-domain luminescent spectroscopy, Physical Review B 78 (2008) 125311.